UNIVERSIDADE DA BEIRA INTERIOR
Engenharia

Experimental Study of a Single Droplet Impinging on Dry Surface with and without a Crossflow: Jet Fuel and Biofuel Mixtures

(Versão corrigida após defesa)

Nuno Filipe Costa Cunha

Dissertação para obtenção do Grau de Mestre em
Engenharia Aeronáutica
(Ciclo de estudos integrado)

Orientador: Prof. Doutor André Resende Rodrigues da Silva

Covilhã, março de 2018

Acknowledgments

I would like to express my gratitude to my supervisor, Dr. André Resende Rodrigues da Silva for the suggestions, dedication, encouragement, and guidance in all stages of this work. My thanks also go to Professor Jorge Manuel Martins Barata for giving me the opportunity to belong and collaborated in the AeroG – Aeronautics and Astronautics Research Center.

My thanks to Dr. Adriana Sousa, Dr. Ilídio Correia, Dr. Sónia Sousa, and Sónia Miguel, for their help in measuring the thermophysical properties of the substances and also to the Laboratory Technician, Rui Manuel Tomé Paulo, for all the help and contribution given in the construction of the experimental facility.

Many thanks to Daniela and Eduardo for their help and suggestions during this work.

Last but not least, I am truly grateful to my family especially to my parents and to Filipa for all their encouragement, dedication, and support gave to me.

Resumo

O impacto de gotas em diferentes superfícies é um fenómeno muito complexo e importante e possui uma variedade de aplicações como sistemas de extinção de fogo, pintura por pulverização, pulverização de culturas e preparação de mistura em motores de combustão interna. Embora estes fenómenos sejam amplamente estudados, o presente trabalho tem como objetivo estudar a influência em misturar um biocombustível num combustível de avião convencional e caracterizar o resultado do impacto de uma gota numa superficie seca com e sem escoamento cruzado. Este estudo permite o desenvolvimento de modelos numéricos para determinar o limite dos diferentes fenómenos de impacto.

Neste estudo, uma instalação experimental foi projetada para estudar o comportamento do impacto de gotas numa superfície de alumínio polida e seca. Foram analisadas quatro substâncias: duas misturas($75\%\ JF$ - $25\%\ HVO$ e $50\%\ JF$ - $50\%\ HVO$) e outras duas substâncias ($100\%\ JF$ e H_2O). O combustível de avião foi usado para comparar o efeito do biocombustível no resultado de impacto, e o H_2O foi usado como substância de controle. Observou-se que as misturas exibem um limite splash/não-splash diferente para a mesma condição inicial, sugerindo que as propriedades do biocombustível influenciam o resultado do impacto. Para estudar o efeito de um escoamento cruzado no impacto de gotas, um túnel de vento também foi projetado. Observou-se que com a aplicação de um escoamento cruzado a gota sobre uma deformnação que parece fazer variar a condição do impacto. Foi realizada uma comparação entre o impacto normal e o impacto com um escoamento cruzado. Foram utilizadas três velocidades para o escoamento cruzado, $7m/s$, $10m/s$ e $15m/s$.

Foram observados diferentes resultados comparando um impacto com um escomento cruzado com um impacto normal e os componentes da velocidade parecem ter algum significado na transição dos fenómenos de impacto. Os resultados foram comparados com alguns critérios de transição propostos na literatura e os resultados do presente estudo indicam que alguns destes podem ser utilizado para outros estudos. Verificou-se também que um estudo da rugosidade superficial da superficie de impacto permitiria tirar mais conclusões.

Palavras-chave

Biocombustível, Motores de Avião, Escoamento cruzado, Gotas, Limite Splash/não-splash

Abstract

The impact of droplets on different surfaces is a very complex and important phenomenon and it has variety of applications such as fire suppression systems, spray painting, crop spraying and blending preparation in internal combustion engines. Although these phenomena are widely studied, the present work aims to study the influence in mixing a biofuel in a conventional jet fuel and characterize the impact result of the droplets in these mixtures. This study allows the development of numerical models to determine the limit of the different impact phenomena.

In this study, an experimental facility was designed to study the droplet impact behavior on a smooth, dry aluminum surface. Four substances were analyzed: two mixtures($75\%\ JF$ - $25\%HVO$ and $50\%\ JF$ - $50\%\ HVO$) and two other substances ($100\%\ JF$ and H_2O). Jet fuel was used to compare the effect of biofuel on the impact result, and H_2O was used as the control substance. It was observed that the blends exhibit a different splash/non splash threshold suggesting that the biofuel properties influence the impact result. To study the effect of a crossflow in this phenomenon, a wind tunnel was also designed and a comparison between normal impact and impact with a crossflow was made. Three crossflow velocities were used and the velocity of the impact was divided into two velocity vectors.

Different results were observed comparing crossflow impact with normal impact and the velocity components seem to have some significance in the transition of the impact phenomena. The results were compared with some transition criteria proposed in the literature and the data indicate that none of them presents a good correlation for the data. It was also verified that a study of the surface roughness of the used plate would allow drawing more conclusions.

Keywords

Biofuel, Aero Engines, Crossflow, Droplets, Splash/non-Splash Threshold

Contents

List of Figures

List of Tables

Nomenclature

a, b	Dependent constants
A, B	Surface roughness coeficient
C_p	Contraction velocity pressure
d	Screen wire diameter
D_0	Droplet diameter before impact
D_{eq}	Inlet equivalent diameter
F	Dimensionless parameter for wall velocity
$G1, G2$	Guillotines that allow controlling the crossflow velocity (1 and 2, respectively)
H	Height
K	Pressure drop coefficient
K_c	Dimensionless splashing parameter
l	Mesh length
L	Nozzle length
La	Laplace number
m	Mass
Oh	Ohnesorge number
Re	Reynolds number
s	Distance between 0.4 C_{pi} and 0.8 C_{pi}
U	Velocity
U_x	Horizontal velocity component
U_y	Vertical velocity component
$\tilde{u_2}$	Exit velocity nonuniformity
V	Volume
We	Weber number
We_c	Critical Weber number
x	Contraction nozzle axial length coordinate
X	Nozzle shape parameter

Greek Symbols

β	Open area ratio
$\triangle h$	Height difference registered in the manometer
$\triangle h_{ref}$	Height difference reference
θ	Impact angle
θ_c	Contact angle
μ	Dynamic viscosity
ν	Kinematic viscosity
ρ	Density
ρ_{air}	Air Density
ρ_{H_2O}	Water Density
σ	Surface tension
τ_s	Surface roughness average height

Subscripts

a	Absolute velocity
e	Maximum
i	Minimum
x	Horizontal coordinate velocity
y	Vertical coordinate velocity
0	Before Impact
1	Inlet
2	Exit

List of Acronyms

ASTM	American Society for Testing and Materials
CI	Crossflow Impact
CR	Contraction Ratio
fps	Frames per second
HEFA	Hydroprocessed Esters and Fatty Acids
HVO	Hydroprocessed Vegetable Oil
JF	Jet Fuel
NEXTBL	Next Generation Biomass-to-Liquid
NI	Normal Impact

Chapter 1

Introduction

This first chapter presents the motivation and the objectives of the present experimental study. A review of the current literature was made to introduce some concepts such as the effect of the incident angle, wall roughness and the effect of a crossflow in a droplet impingement on a dry surface. Some deposition/splash transition criteria proposed in the literature which are also presented in this section.

1.1 Motivation

The constant increase in oil prices and the application of environmental targets in various countries escalated the pursuit to create cleaner and more efficient energy production. Normally it takes years of intense testing and high funding until the appliance of the new systems for cleaner energy production is finished.

To bypass this problem the present study aims to successfully applied biofuels to low emission aero engines combustors. At the same time, this would decrease costs and reduce greenhouse gases emissions. Also, current legislation allows the use of biofuels in the aeronautical industry. As it was mentioned in Pizziol [7], the stander specification ASTM D7566 defines that the maximum blending ratio allowed for HEFA (Hydroprocessed Esters and Fatty Acids) type alternative fuels is $50\ \%$ in volume. The biofuel used in this study is a HEFA type alternative fuel, which is known under the commercial name of NEXTBL (Next Generation Biomass-to-Liquid). In the present work the biofuel used is called HVO (Hydroprocessed Vegetable Oil) which is also the name given to HEFA type fuels where animal biomass is not involved [7].

To be able to apply this substance in aero engines combustors, the thermophysical properties on droplet atomization and the characterization of droplet/spray impingement processes needed to be studied. For this, the design and construction of an experimental facility was required.

1.2 Literature Review

1.2.1 Droplet/Wall Interactions

The behavior of droplets impacting on dry surfaces is not fully understood. It involves a number of influencing parameters and the outcomes are normally classified by observing the morphological characteristics of the impinging drop. In his experimental work, Riobbo et al. [6] identify six possible outcomes for droplet impact on dry surfaces: deposition, prompt splash, corona splash, receding breakup, partial rebound and rebound (shown in figure 1.1).

Deposition occurs when the drop impacts on the surface and only suffers deformation. Impacting with the surface, the droplet will spread out and formed what is called a lamella with a visible outer rim. When this lamella reaches the maximum spreading diameter it recoils and forms a liquid film over the surface. For high Weber and Reynolds numbers, prompt splash may occur and

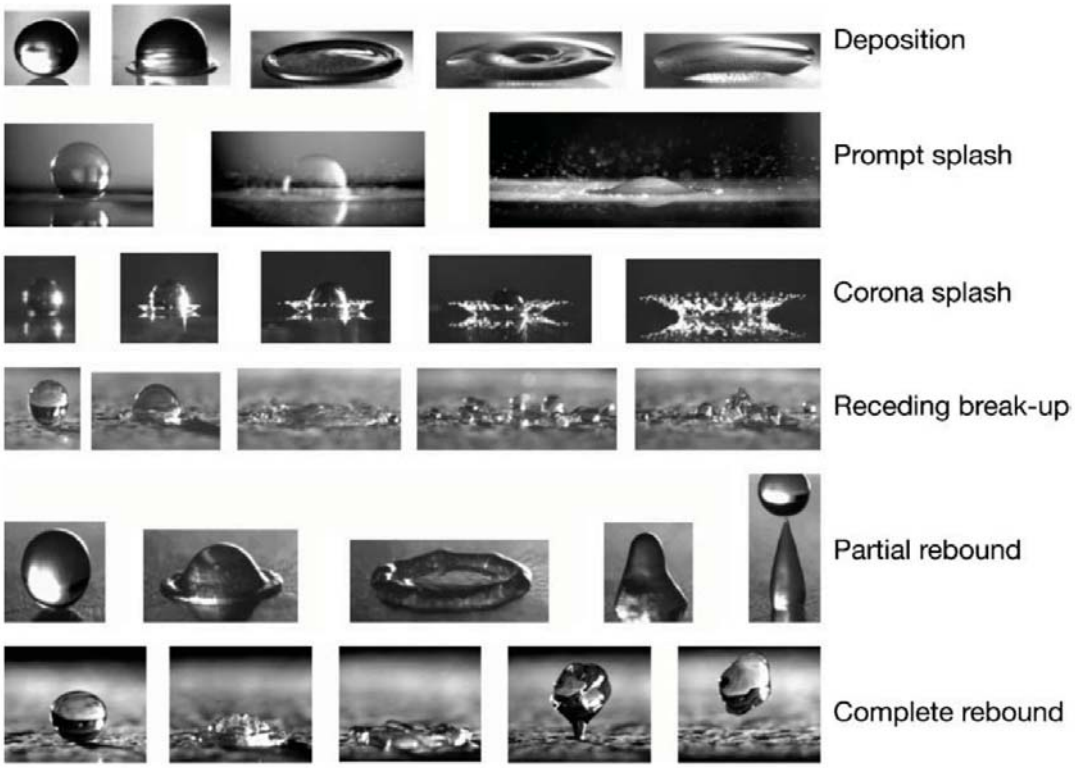

Figure 1.1: Morphology of drop impact on a dry surface [1].

this impact happens when smaller droplets are ejected from the impact region. Corona splash is observed when a drop impacts with sufficient velocity so the outer rim formed by the lamella has sufficient energy that elevates and creates a crown-like shape. When it reaches the maximum crown height smaller droplets separate from this shape. This phenomenon is also referred as crown splash [8]. Although both phenomena described the occurrence of splash, the prompt splash does not present a crown-like shape. Furthermore, the secondary atomization occurs in different stages for both phenomena. The receding breakup occurs after the spreading of the droplet. It happens if, when the lamella starts to recede after the maximum spreading diameter is reached, the dynamic contact angle reaches zero. Then, some droplets are left behind. The partial rebound and complete rebound depend on the contact angle and the maximum diameter reached. It only happens if a receding phase is observed. For high energy impacts, during the receding phase, not all energy is dissipated and if that energy reaches the impact point the fluid is elevated. During the receding phase, the contact angle will define if a partial rebound (low contact angles) or a complete rebound (high contact angles) happens . Moita and Moreira [9] also reported the occurrence of finger breakup, this phenomenon was encountered at moderate impact velocities and is an early consequence of some instabilities during the spreading phase. When the lamella is spreading, some fingers-like shape structures are created and break up in the final stage of spreading. This fingering phenomenon is also described by Yarin [8].

The outcome of a droplet impact on a solid surface is governed by a number of parameters such as droplet velocity, size, impact angle, fluid properties(viscosity, surface tension), surface roughness and even if a gas boundary layer is applied in the near-wall region [3].

The relative magnitude of the different types of forces involved in the impact is normally presented as dimensionless numbers. This numbers can be used to predict the outcome of a drop

impact. The dimensionless numbers employed in this work are:

1. The Weber number (We), relates the inertial forces with the surface tension forces.

$$We = \frac{\rho U_0^2 D_0}{\sigma} \quad (1.1)$$

2. The Reynolds number (Re), relates the inertial forces with the viscous forces.

$$Re = \frac{\rho U_0 D_0}{\mu} \quad (1.2)$$

3. The Ohnesorge number (Oh), relates viscous forces to inertial and surface tension forces.

$$Oh = \frac{\sqrt{We}}{Re} = \frac{\mu}{\sqrt{\rho \sigma D_0}} \quad (1.3)$$

4. The Laplace number (La), measures the relative importance of surface tension and viscous forces acting on the liquid.

$$La = \frac{\rho \sigma D_0}{\mu^2} \quad (1.4)$$

Where D_0 and U_0 represent the diameter and the velocity of the droplet before impact. And ρ, σ and μ are the liquid density, surface tension and viscosity, respectively.

The impact angle (θ) is formed by the angle formed between the absolute velocity vector of the incident droplet and the impact surface (figure 1.2).

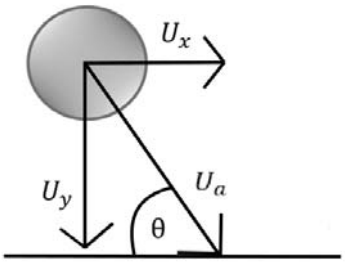

Figure 1.2: Velocity vectors and impact angle representation.

Jayaratne and Mason [10] find that the droplets outcomes depend on the impact angle. This angle also influences the direction of the secondary droplets for smooth surfaces. A small incident angle of the droplet leads to a small reflection angle, while a large incident angle leads to a large deflection angle [4]. According to Yao and Cai [11] if the impact angle is not 90 °, the tangential velocity of the droplet destabilizes the liquid film and enhances the fragmentation of the droplet following the impingement.

It is worth mention that impact angle differs from contact angle (θ_c). The contact angle is influenced by the liquid properties and the surface topography. When a droplet impacts on a solid surface, a liquid film is formed, and due to the influence of the surface tension and surface forces, this film reaches a maximum diameter and then recoils. When this process reaches equilibrium the contact angle can be measured. This angle is also known as wettability

of the surface [12]. If a wetted surface is presented, the contact angle will vary between 90º and 180º and if a non-wetted surface is presented between 0 ºand 90 º (figure 1.3) [2].

Figure 1.3: Contact angle representation (adapted from [2]).

The surface roughness is also an important parameter in the droplets impingement dynamics [4], [13], [14], [15] and it is normally characterized by its average height (τ_s). Mundo et al. [4] observed that the surface roughness alters the impact angle of impinging droplets. For small droplets, this effect becomes more evident. This also affects the volume, number, and the size distribution of secondary droplets. For rough surfaces, the critical threshold for splash is lowered in relation to smooth surfaces [1]. Also, the mass of the splash decreases with the increase of surface roughness [13].

Mundo et al. [13] also showed that the droplets with high kinetic energy presented a more irregular behavior for rough surfaces compared to smooth surfaces. For rough surfaces, the high tangential momentum leads to disintegration into secondary droplets and the normal phenomena are no longer observed. Droplets with low kinetic energy impacting in rough surfaces did not present different results for those impacted on smooth surfaces. The droplet deposits and spread out forming a liquid film (deposition) and in this case, the surface roughness does not promote splashing of the primary droplet.

For smooth surfaces, the diameter distributions of secondary droplets depend on the fluid properties and kinematic parameters. For rough surfaces, the secondary droplets have smaller mean diameters and smaller diameter distribution [4].

Table 1.1: Influence of different parameters on the impact outcome (adapted from [6]).

An increase of	Deposition	Prompt Splash	Receding Breakup	Complete Rebound	Crown Splash	Partial Rebound
U_0	↓	↑	↑		↑	↑
D_0	↓	↑				
σ		↓	↑	↑	↓	↑
μ	↑	↓	↓		↓	
τ_s	↓	↑			↓	
θ_c			↑	↑		↑

There are other parameters that affect the dynamic behavior of the droplets prior to impact, namely a crossflow. This crossflow affects the direction and the outcome of droplets before impact [16]. The effect of a crossflow on the impingement droplets can be attributed to aerodynamic forces exerted by the gas flow. When the droplet enters the gas flow it may deform and be oriented by the direction of the flow. This flow will also apply an additional force to the droplet which can vary the outcome of the impingement [17]. The secondary atomization dynamics also can be affected by the crossflow [18], [19].

The temperature, the presence of a liquid film in the surface can also alter the outcome of droplet impact, however, they are not variables in the present study.

Riobbo et al. [6] presented a correlation between the parameters and the outcomes of the impingement phenomena. Table 1.1 presents this correlation where the upward arrow and the

downward arrow represent an increase and a decrease, respectively, in the importance of the variable in the impact outcome.

1.2.2 Deposition/Splash Transition Criteria

The outcome of a droplet impinging on a wall depends on a number of conditions. To be able to establish the transition criteria between impingement regimes a number of empirical correlations has been proposed. These correlations determine the limit between different impact phenomena and are used to describe how a droplet will behave on the surface.
In the literature, the Reynolds number, Weber number, Ohnesorge number, and Laplace number are used in these models. Stow and Hadfield [15] presented the splashing parameter (K_c) which is used to determine when splash occurs. It is defined as:

$$K_c = B.Oh^a.We^b \quad (1.5)$$

Where a and b depend on the experimental conditions. This relation dictates that the transition between the different regimes occurs when the dimensionless parameters become critical. The numerical value for this threshold depends on size, velocity, temperature, incident angle and fluid properties, as well as different wall conditions; wall temperature, relative film thickness, surface roughness [17]. There is a variety of models in the literature, however, in the present work, only three could be applied.

In Bai and Gosman [3] work, different impinging regimes were identified for dry and wetted walls depending on the Weber number and wall roughness. For dry surfaces, the empirical correlation was derived from data in Stow and Hadfield [15] experiment and in this correlation, the surface roughness was considered. The A coefficient depends on the surface roughness and table 1.2 shows the different values of the A coefficient proposed. Equation 1.6 presents the criterion proposed, and if the critical Weber number (We_c) is reached splash occurs.

$$We_c = A.La^{-0.18} \quad (1.6)$$

Table 1.2: Typical values of A depending on the surface roughness (adapted from [3]).

τ_s [µm]	A
0.05	5264
0.14	4534
0.84	2634
3.1	2056
12	1322

The model presented by Mundo et al [13] uses the splashing parameter (K_c) to define the transition criteria. Their experiment shows that the critical point where deposition transitioned to splash was $K = 57.7$. This means that when K was below 57.7 the droplet would deposit on the surface, and when it was above, splash would occur. This study was made with two different surfaces.It used two discs, one with a smooth surface and the other with a rough surface. Also, the collision angle and the impingement velocity where determined by the rotational speed of the disc. The following equation (1.7) presents the boundary limit for this criteria:

$$Oh.Re^{1.25} = 57.7 \quad (1.7)$$

The last correlation used in the present work was proposed by Randy et al. [5] who used a large number of hydrocarbon fuels and alcohols to develop their criteria. Although Randy et al. [8] observed different disintegration mechanisms, a single threshold was developed to fit all their data. This correlation fitted well with their experimental results for high Reynolds numbers, however, when viscous forces and wettability effects became more significant (lower Reynolds numbers) the data did not fit well with this correlation. This experiment was conducted with an aluminum disk with very low surface roughness. Equation 1.8 presets the transition criteria proposed:

$$Oh.Re^{0.609} = 0.85 \quad (1.8)$$

1.3 Objectives

This study aims to analyse the impact phenomena of mixtures of biofuel and conventional jet fuel. To accomplish this goal, it was design and constructed an experimental facility to study the behavior of a single droplet impinging on a dry surface with and without a crossflow. A wind tunnel was designed to study the difference between normal impact and the impact with a crossflow. The droplet was exposed to the influence of three different crossflow velocities (7, 10 and 15 m/s). This facility allowed to visualize the different impact phenomena of the droplets and identify the different impact regimes.

Four substances were used: $100\%\ JF$, $75\%\ JF$ and $25\%\ HVO$, $50\%\ JF$ and $50\%\ HVO$ and H_2O. Water (H_2O) is an extensively studied fluid and is used as a reference substance. Comparing the results of the two mixtures with $100\%\ JF$, the influence of adding the biofuel will be analyzed.

Lastly, the results were compared to the transition criteria.

Chapter 2

Experimental Study

In this chapter is described the experimental facility and the procedure of the experimental study. First, it's presented the wind tunnel construction and calibration. Then, it's showed the injection system, and the image acquisition system used in this work and also some characteristics of the working fluids are presented to better understand some results. Finally, a description of how the image analysis is made and some results are presented.

2.1 Experimental Facility

Figure 2.1: Experimental facility.

A schematic image of the experimental facility is presented in figure 2.1. A ventilator with 15 kW was used to provide a crossflow with 3000 m^3/h through a low-speed wind tunnel. The wind tunnel has a rectangular exit nozzle with $200{\times}40$ mm^2 and the impact surface is a smooth aluminum plate with $700{\times}80$ mm^2. This plate is placed across the exit nozzle and is equidistant to two glasses, one of which is a diffusion glass used to spread the light evenly. The light is provided by a $20W$ Led light and is aligned with the impact surface and directly across from the high-speed camera.

2.1.1 Wind Tunnel Design

2.1.1.1 Diffuser

The diffuser is used to decelerate the crossflow and typically they have angles below $7,5$ °, however, that would require a long diffuser [20]. Due to a lack of space, a small one was used, and in this case, separation may occur. To avoid this, a screen was placed where the

diffuser's angle suffers a sudden change removing the direct effects of layer growth and incident separation [21]. The diffuser used has a length of $335\ mm$ and its angle is about 48.24 °. It has $100\ mm$ square inlet and a $40\times400\ mm$ exit nozzle. In the present work this diffuser was already built and the following parts of the wind tunnel were built considering its characteristics.

2.1.1.2 Settling Chamber

According to Mehta and Bradshaw [21], the settling chamber consists of two components: honeycomb, and screens. The honeycombs are effective to remove swirl and lateral mean velocity variations, providing that the flow yaw angles are lower than 10 °. This section of the settling chamber was already constructed and was only verify that the cell length of the honeycombs was 6 to 8 times its diameter in order to maximize the overall benefit.

The next step was to place the screens, imposing a static pressure drop proportional to U^2. This allows a more uniform velocity profile of the flow and reduces the boundary layer thickness, giving the flow an increased ability to withstand a pressure gradient. Variations in the longitudinal mean velocity are nearly all removed by a screen with a pressure drop coefficient of 2.

There are some parameters to take into account in order to build a settling chamber, the pressure drop coefficient K that needs to have a value of 1.5 in order to reduce the yaw and swirl angles of about 40º with a factor of about 0.7, and the open area ratio , that needs to be higher than 0.57 if a two-dimensional boundary layer without instabilities is required. In order to fulfill these principles, the first screen should be placed at the beginning of the settling chamber and since there was a range of velocities in this work it was dimensioned for the highest velocity expected. With the decrease in velocity, the pressure drop coefficient K increases, so for lower velocities this screens still fulfills its purpose. In order to calculate this two variables the following equations were used [22]:

$$\beta = \left(1 - \frac{d}{l}\right)^2 \quad \text{(2.1)}$$

$$K = 6.5\frac{1-\beta}{\beta^2}\left(\frac{Ud}{\beta\nu}\right)^{-\frac{1}{3}} \quad \text{(2.2)}$$

where d is the screen wire diameter and l the mesh length.
The next step was to calculate the spacing between screens, and for this two proprieties should be considered [21]:

1. The spacing between screens must be enough for the static pressure fully recover from a perturbation before reaching the next screen;

2. The minimum spacing, for the turbulent-reduction point of view, should be the magnitude of the eddy containing the maximum energy.

It was also found that 20 % of the settling chamber diameter performs successfully [21]. Also, the distance between the last screen and the contraction entry should be the same, being that if it is a shorter distance significant distortion of the flow should be expected.Table 2.1 summarizes the characteristics of the settling chamber, figure 2.2 shows the schematic of the wind tunnel

to visualize the location of the screens and figure 2.3 shows the settling chamber used in the present work.

Table 2.1: Design parameters of the settling chamber.

Section Area (height x width) [mm]		400 x 40
Area [m^2]		0.016
Equivalent Diameter [mm]		142.7
Honeycombs	Cell Area [mm^2]	26.0
	Cell Diameter [mm]	6.00
	Cell Lenght [mm]	48.0
Screens	d [mm]	0.25
	l [mm]	1.34
	β	0.67
	K	$\approx$ 1.80
Spacing between screens [mm]		30

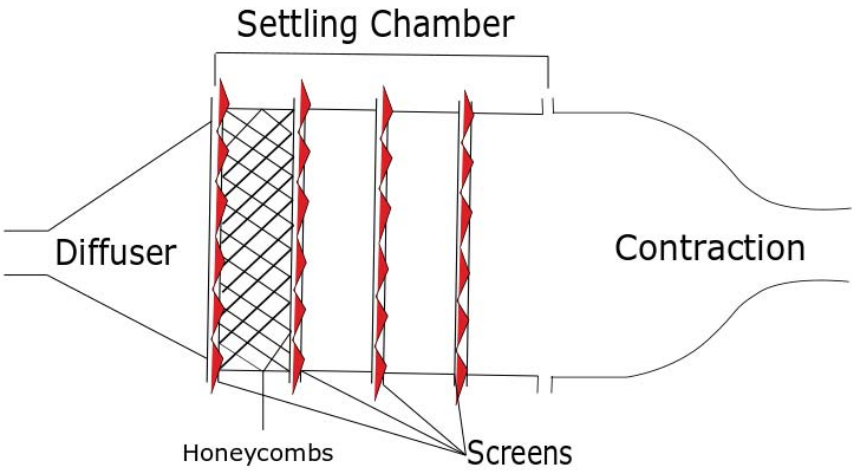

Figure 2.2: Schematic of the screens placing.

Figure 2.3: Settling Chamber.

2.1.1.3 Contraction

The contraction is used to accelerate the flow allowing the placement of the screens and honeycombs in a low-speed area reducing pressure losses. The length of the contraction is an important factor given that if it is long enough it would be possible to avoid separation, however, besides the space requirements, this would increase the exit boundary layer thickness[21]. The procedure used to design this section of the wind tunnel was a numerical method suggested by Thomas Morel [23] where the shape of the wall is constituted by two cubic arcs join smoothly. The main criteria to create this section were to guaranteed an uniformity of the exit flow and avoid separation. After choosing the contraction ratio (*CR*) there are two important coefficients to be assumed in order to avoid separation *Cpi*, and *Cpe*, defined as:

$$Cpi = 1 - \left(\frac{V_i}{U_{1,\infty}}\right)^2 \quad (2.3)$$

$$Cpe = 1 - \left(\frac{U_{2,\infty}}{V_e}\right)^2 \quad (2.4)$$

Where *i* and *e* represent the point of minimum and maximum wall velocity, and *1* and *2* correspond to the inlet and exit flow velocities, respectively. The next step was to determinate the two dimensionless parameter *Fi* and *Fe* and calculate the nozzle shape parameter defined as:

$$X = \left[1 + \frac{1}{CR}\left(\frac{Fi}{Fe}\right)^{\frac{1}{2}}\right]^{-1} \quad (2.5)$$

which represents the match point of the two cubic arcs. To calculate the nozzle length one of the following equation was used:

$$Fi = \frac{CR-1}{CR} X^{-2} \left(\frac{L}{H_1}\right)^{-3} \quad (2.6)$$

$$Fe = \frac{CR-1}{CR^3} (1-X)^{-2} \left(\frac{L}{H_1}\right)^{-3} \quad (2.7)$$

And the contour of the contraction was defined by:

$$\frac{H-H_2}{H_1-H_2} = 1 - \frac{1}{X^2}\frac{x^3}{L^3}, \qquad \frac{x}{L} \leq X \quad (2.8)$$

$$\frac{H-H_2}{H_1-H_2} = \frac{1}{(1-X)^2}\left(1-\frac{x}{L}\right)^3, \qquad \frac{x}{L} > X \quad (2.9)$$

Where H_1 and H_2 represent the inlet height and the exit height respectively and x the length coordinate. According to the Stratford separation criteria for turbulent flow [24], the *Cpi* value

was obtained using:

$$Cpi = 0.7 \left(\frac{\frac{x_0}{H_1} + 0.9\frac{x_i}{H_1}}{\frac{s}{H_1}} \right)^{-\frac{1}{3}} \left(10^{-6} Re_x\right)^{\frac{1}{15}} \quad \textbf{(2.10)}$$

$$Re_x = \frac{U_{1,\infty}}{H_1} \frac{\frac{x_0}{H_1} + 0.9\frac{x_i}{H_1}}{\nu} = O\left(10^6\right) \quad \textbf{(2.11)}$$

An iterative method was used where s is the distance between 0.8 and 0.4 of *Cpi* and x_0 is the distance from the virtual origin of a boundary layer to the nozzle beginning and x_i represents the axial coordinate for the minimum wall-velocity. T. Morel [23] suggested 0.3 as a typical value of the ratio between x_0 and H and the remaining ratios were taken from his graphics. The exit velocity nonuniformity is given by:

$$\tilde{u_2} = (0.19 \pm 0.01)\, Cpe \quad \textbf{(2.12)}$$

It is proportional to *Cpe* when is less than 0.1 and it will ensure that the nonuniformity of the velocity distribution at the exit will not be more than 2 %.It is also suggested that the last screen should be placed at a distance of 0.2 of the inlet equivalent diameter (D_{eq_i}), so, the "total" nozzle length is the sum of $0,2\ D_{eq_i}$ and L.
Table 2.2 summarizes the characteristics of the contraction shown in figure 2.4.

Table 2.2: Parameters of the contraction design.

Contraction Ratio CR	2
Cpi	0.285
Cpe	0.058
H_1 Inlet height [mm]	400
H_2 Outlet height [mm]	200
X	0.423
L Lenght [mm]	482.2
"Total" nozzle lenght [mm]	512.2
Width [mm]	40

Figure 2.4: Wind tunnel contraction ($CR = 2$).

2.1.2 Calibration

The calibration of the crossflow was made by adjusting two guillotines (G_1,G_2), shown in figure 2.5, that allowed air to pass through the wind tunnel. The measurements of the velocity values were made through a pitot tube that was placed at $1\ cm$ of the nozzle exit. This was connected to a U-shaped manometer and registered the difference between the total pressure and the static pressure ($\propto \triangle h$) with an error of $\pm 0.5\ mm$. The velocity (U) was calculated using equation 2.13.

$$\frac{1}{2} \times \rho_{air} \times U^2 = \rho_{H_2O} \times g \times \triangle h \Longleftrightarrow U = \sqrt{\frac{2 \times \rho_{H_2O} \times g \times (\triangle h)}{\rho_{air}}} \quad (2.13)$$

Figure 2.5: Guillotines representation.

The position of the guillotines for the desired velocities was not known so, five tests were performed in order to verify the position in which would obtain a greater velocity range. Table 2.3 shows the positions taken by the guillotines and figure 2.6 illustrates the results.

Table 2.3: Calibration tests.

Test A		Test B		Test C		Test D		Test E	
$G_1[mm]$	$G_2[mm]$	$G_1[mm]$	$G_2[mm]$	$G_1[mm]$	$G_2[mm]$	$G_1[mm]$	$G_2[mm]$	$G_1[mm]$	$G_2[mm]$
0	140	35	140	70	140	105	140	140	140
0	105	35	105	70	105	105	105	140	105
0	70	35	70	70	70	105	70	140	70
0	35	35	35	70	35	105	35	140	35

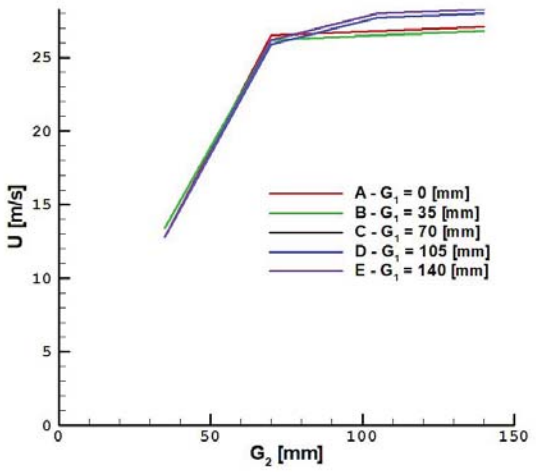

Figure 2.6: Calibration chart.

As it is possible to observe through figure 2.6, test E is the one that has a greater velocity range. In this way, the variation of the crossflow will be made only with the G_2 having G_1 always open. In planning the experimental study it was defined that three velocities would be studied: $7m/s$ $10m/s$ $15m/s$. To obtain these velocities it was necessary to draw a chart that relates the velocity of the wind tunnel with the position of G_2 (figure 2.7), and an equation was obtained. In order to guarantee the velocities for the experimental study, a tube was placed in the inlet of the crossflow before the diffuser and the static pressure was measured whit a manometer so a relation could be achieved between the velocities in the working section and in this reference. Table 2.4 shows the water column millimeters obtained for the velocities in these two positions.

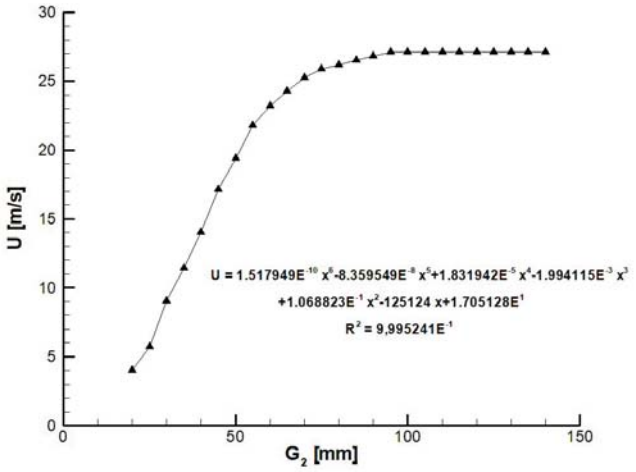

Figure 2.7: Velocity obtained by varying G_2.

Table 2.4: Velocities used in this study.

U $[m/s]$	$\triangle h_{ref}$ $[mm]$	$\triangle h$ $[mm]$
7	6	3
10	14	7
15	25	14

Since the contraction was made in the workshop, it was necessary to draw the velocity profile at the nozzle exit. Five points were chosen vertically and a $5mm$ spacing was used horizontally and the velocity profiles were measured. Figure 2.8 shows a schematic of the points(at blue) where the velocities were measured. The red line is a representation of the position of the velocity profiles. Figures 2.9 and 2.10 present the horizontal and vertical velocity profiles, respectively. To guarantee a stable crossflow influence the aluminum plate was placed $70\ mm$ above the base of the exit nozzle.

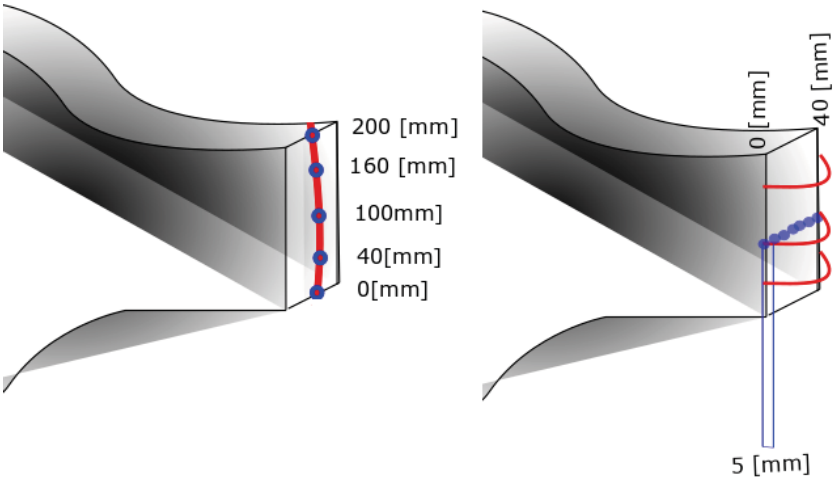

Figure 2.8: Schematic for velocity profiles measurements (vertically to the left and horizontally to the right).

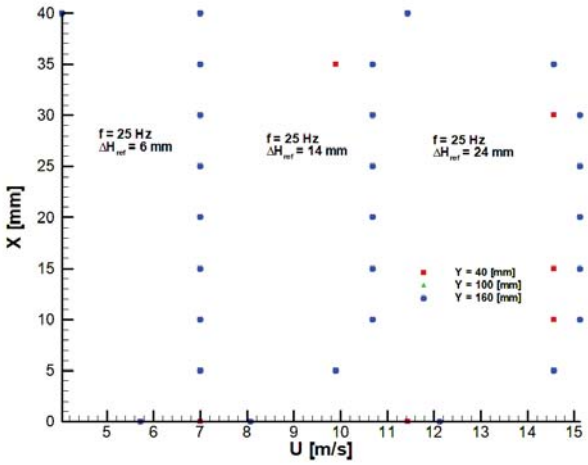

Figure 2.9: Horizontal velocity measures.

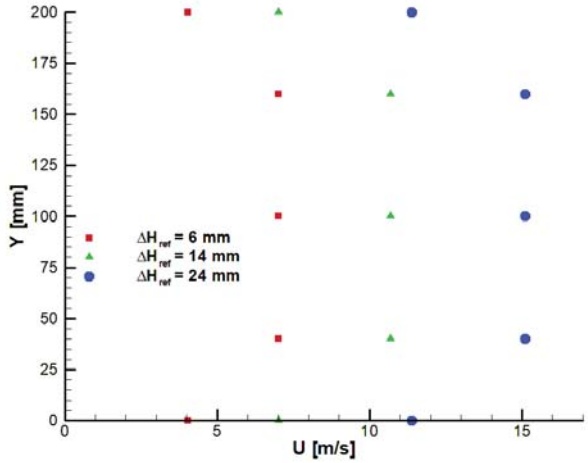

Figure 2.10: Vertical velocity measures.

2.1.3 Injection System

The injection system is constituted by an NE-1000 Single Syringe Pump (figure 2.11), with a pumping rate of 1.459 µl/hr for a $1\ ml$ syringe, or $127.2\ ml/min$ for a $60\ ml$ syringe. For this work was used a $50\ ml$ syringe with a diameter of $28.0\ mm$. The pumping rate was established at $0.5\ ml/min$ and the syringe was connected to a needle with an inner diameter of $1.50\ mm$. These characteristics allow that there is practically no acceleration given to the droplet by the injection system allowing the droplet to drop by the force of gravity.

Table 2.5 shows the working conditions used in this experimental work being D_0 the droplet's diameter and U_0 the droplet velocity before impact. The other four represent the dimensionless numbers: Reynolds, Weber, Ohnesorge and Laplace.

Figure 2.11: NE-1000 Single Syringe Pump.

Table 2.5: Range of values from the experimental work.

D_0 [mm]	3.02	4.06
U_0 [m/s]	1.78	4.76
Re	3656	19232
We	389	1277
Oh$\times 10^3$	1.846	7.311
La	18708	293454

2.1.4 Image Acquisition System

A high-speed camera, FASTCAM mini UX50, was used to capture the motion of the droplets. It has a 1.3 megapixel image resolution at frame rates up to $2000\ fps$ (frames per second) and it can go up to $160000\ fps$ with a resolution reduction. Also, a Macro Lens Tokina AT-X M100 AF PRO D with a minimum focus distance of $300\ mm$, a focal length of $100\ mm$, a 1:1 macro ratio and a filter size of $55\ mm$. In order to be able to observe some of the phenomena, some characteristics were changed, the resolution was reduced to increase the number of images captured (higher fps) and the shutter was also increase given that some of the droplets reached velocities that blurred the images. By decreasing the shutter to $1/10240$ s the exposer time was decreased, and the blurred image problem was solved. Therefore, in this study images were taken with a frame rate of $10000\ fps$ and a shutter of $1/10240$ s. However, by decreasing the shutter, the image becomes darker because the exposer time is smaller. This is shown in figure 2.12 and figure 2.13.

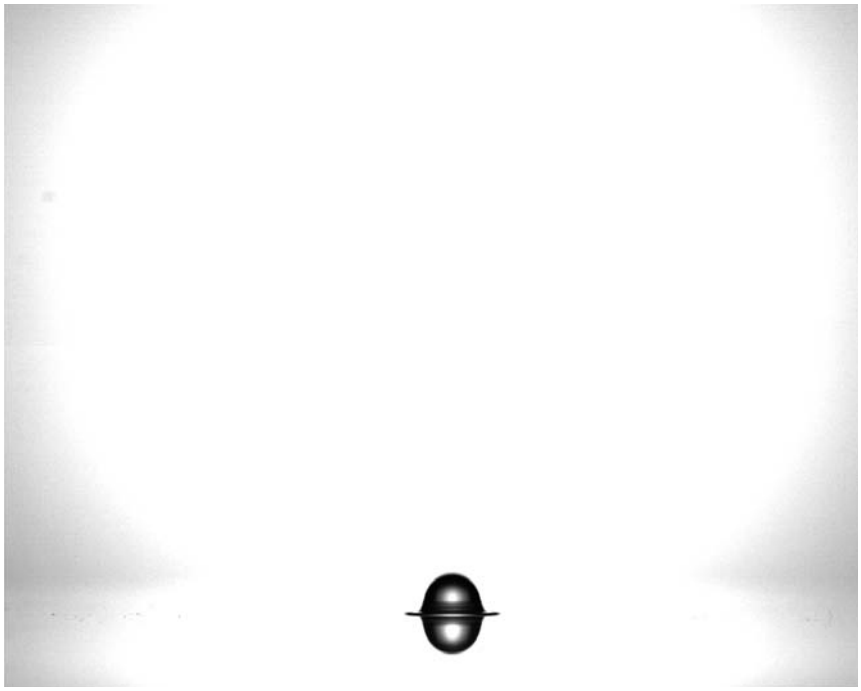

Figure 2.12: Image with 1280x1024 resolution and $1/5120$ s shutter.

Figure 2.13: Image with 240x1024 resolution and $1/10240$ s shutter.

The camera was connected to a computer and the images were manually taken whit the help of a trigger.

2.2 Work Fluids Properties

The experimental work aims to study the characteristics of biofuel droplets and, for that purpose, the first step was to study the physical proprieties of these substances. The parameters of the experimental study only allow for the study of $100\%\ JF$, $75\%\ JF$ and $25\%\ HVO$, $50\%\ JF$ and $50\%\ HVO$ and H_2O as a control substance, however, for the study of the physical proprieties, it was of interest also examine $75\%\ HVO$ and $25\%\ JF$ and $100\%\ HVO$.

2.2.1 Density

The density (ρ) of a fluid is defined as the mass of the fluid per unit volume [25]. To determine the density, the pycnometer method was used. This method uses a pycnometer (figure 2.14), with a known volume of $25\ ml$, and the mass of the same was measured, with and without the substance. These two are subtracted and the substance's mass is calculated. The precision scale used was a Mettler Toledo PB303 DeltaRange with an error of $\pm 0.01\ g$ and the density was calculated by the equation 2.14.

$$\rho = \frac{m}{V} \quad (2.14)$$

Figure 2.14: Pycnometers used.

For each substance, two tests were made and the mean value was calculated. This work was performed at a temperature of $20°\ C$ and at a 50% humidity. Table 2.6 illustrates the results.

Table 2.6: Results of the tests performed to determine the density of the substances.

Substance	Test number	m [g]	ρ [g/ml]	ρ [kg/m^3]	$\bar{\rho}$ [kg/m^3]
100 % JF	1	19.9503	0.7980	798.0	798.3
	2	19.9639	0.7986	798.6	
75 % JF - 25 % HVO	1	19.8692	0.7948	794.8	795.0
	2	19.8780	0.7951	795.1	
50 % JF - 50 % HVO	1	19.8046	0.7922	792.2	792.4
	2	19.8123	0.7925	792.5	
25 % JF - 75 % HVO	1	19.7479	0.7899	789.9	789.5
	2	19.7491	0.7890	789.0	
100 % HVO	1	19.6090	0.7844	784.4	785.1
	2	19.6470	0.7859	785.9	

2.2.2 Surface Tension

The pendant droplet method was used to determine the surface tension (σ) of the substances, and a Data Physics – OCAH200 (figure 2.15) recently calibrated with a 0.6% accuracy was use. This study consists in capturing an image of a droplet that hangs on a needle and analyzing it with the Data Physics SCA20 software. This software analyses the droplet shape, base on the Young-Laplace's equation that describes the pressure difference between the areas inside and outside of a curved, liquid surface [25]. This work was performed at a temperature of $20°\ C$ and at a 50% humidity and the results are presented in table 2.7.

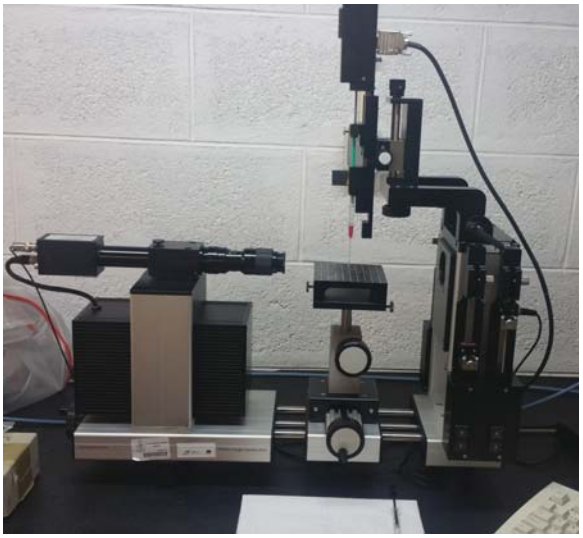

Figure 2.15: Data Physics – OCAH200.

Table 2.7: Surface tension tests results.

Substance	Test 1 [mN/m]	Test 2 [mN/m]	Test 3 [mN/m]	$\bar{\sigma}$[mN/m]
100 % JF	25.49	25.49	25.13	25.37
75 % JF - 25 % HVO	25.55	25.54	25.51	25.53
50 % JF - 50 % HVO	24.6	24.58	24.73	24.64
25 % JF - 75 % HVO	26.61	26.58	26.59	26.59
100 % HVO	26.54	26.61	26.62	26.59

2.2.3 Viscosity

To measure the viscosity a Brookfield DV3T RVCP Rheometer (figure 2.16) with a cone and plate geometry (figure 2.17) for small samples was used. This instrument was used to measure the dynamic viscosity (μ) and has an accuracy of $\pm 1.0\ \%$ of the range. RheocalcT software was used to control the rheometer from a computer. The instrument only measured the dynamic viscosity, however, the kinematic viscosity (ν) was obtained dividing the dynamic viscosity by the density of the substances. This work was performed at a temperature of $23^{\circ}\ C$ and table 2.8 show the results of these tests.

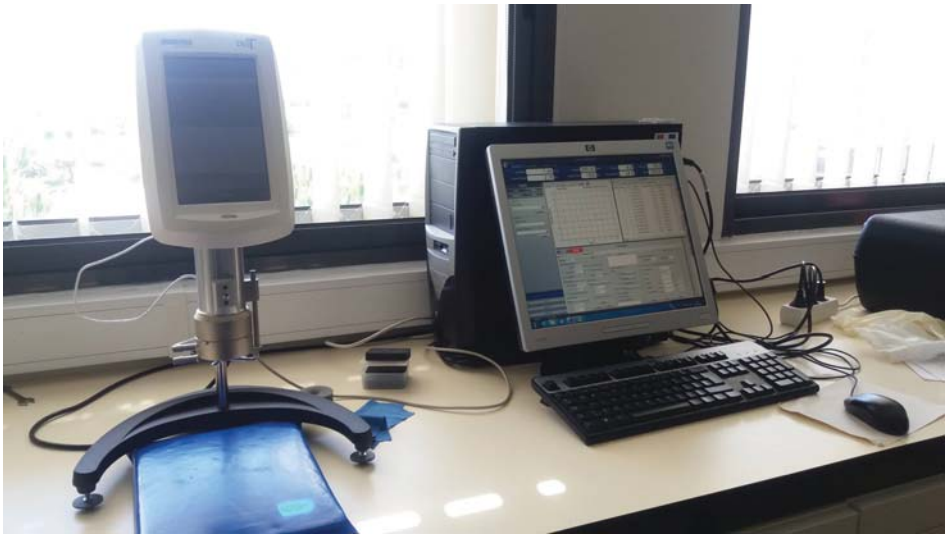

Figure 2.16: Brookfield DV3T RVCP Rheometer (on the left).

Figure 2.17: Cone and plate geometry.

Table 2.8: Viscosity tests results.

Substance	μ $[Pa.s]$	ρ $[kg/m^3]$	ν $[mm^2/s]$
100 % JF	0.00112	798.3	1.403
75 % JF - 25 % HVO	0.00144	795.0	1.811
50 % JF - 50 % HVO	0.00179	792.4	2.259
25 % JF - 75 % HVO	0.00267	790.0	3.380
100 % HVO	0.00340	785.2	4.330

2.2.4 Summary of Work Fluids Properties

Table 2.9 presents, in the form of a summary, the properties of the substances that are used in the experimental study. The control substance (H_2O) is included in this table because it is one of the substances used in the experimental study, however, its properties are reported in the literature.

Table 2.9: Work Fluids Properties.

Substance	ρ [kg/m^3]	σ [N/m]	μ [$Pa.s$]
100 % JF	798.3	0.02537	0.00112
75 % JF - 25 % HVO	795.0	0.02553	0.00144
50 % JF - 50 % HVO	792.4	0.02464	0.00179
H_2O	1000	0.07280	0.00100

2.3 Image Data Processing

The quantitative characterization of some characteristics of the droplets, as the diameter and the impact velocity, were made through image data processing. As it was mentioned before, the images were captured by a high-speed camera and it was necessary to ensure a good image quality to be able to obtain accurate measurements. For processing the captured images an algorithm was developed using Matlab Software.

Figure 2.18 is an example of a typical image of $75\%\ JF$ - $25\%\ HVO$ impact, and its background. Using this two images, we are allowed to calculate the droplets characteristics.

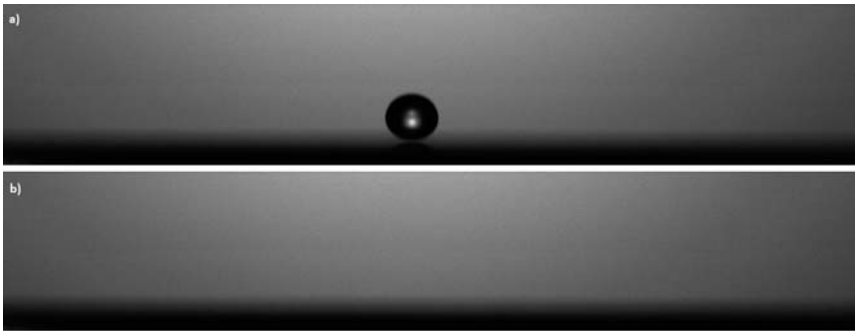

Figure 2.18: Image of an $75\%\ JF$ - $25\%\ HVO$ impact (a) and its background (b).

In Matlab images are essentially a matrix of pixels $[colums, rows]$, having each pixel a value, which in this case, varies between 0 e 3533. Having these two images, the first step was to subtract the image in study, with the background. This will leave in the final image only the pixel values that are different in the two images, that is, the droplet's pixels (Figure 2.19).

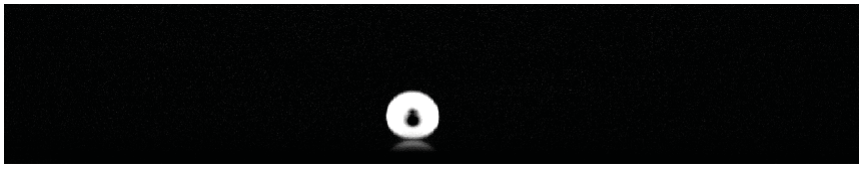

Figure 2.19: Result from image subtraction (with contrast alteration for visualization purposes).

After subtracting the two images a function was used to convert the pixel values to binary values,

being every value 1 shown in white and 0 shown in black. Figure 2.20 shows the binary image created where the white pixels represent the droplet and the black ones the background.

Figure 2.20: Resulting binary image.

How it is possible to observe in figure 2.20 the image possesses black pixels inside the droplet's section, so, a function was used that changes from 0 to 1, every black pixel, or a set of black pixels, that was completely surrounded by white pixels (figure 2.21).

Figure 2.21: Resulting image of changing values of 0 surrounded by values of 1.

Despite all this, the image was not ready to be analyzed, it was still possible to observe some white pixels scatter around. Then, another function was used to remove those white pixels without removing the ones from the droplet's section. This function, unlike the one previously mentioned, changed the pixel value from 1 to 0 of all pixels isolated or grouped into sets smaller than 50 pixels(figure 2.22).

Figure 2.22: Resulting image of changing values of 1 to 0.

To determine the droplet diameter, a function was used to calculate the biggest number of white pixels (1) for the rows and also for the columns. The biggest value obtained represents the droplet diameter in pixels.

Having the droplets diameter in pixels, it was needed to known the value of one pixel in millimeters. Thus, in the beginning of every test, an image of an object was taken that would be used as a reference for the conversion from pixel to millimeter. In this study, a needle (figure 2.23) was used as this reference and the same image processing was applied thus obtaining the diameter, in pixels, of the needle. Measuring the needle's diameter with a digital caliper, the diameter was obtained in millimeters. Obtaining the value of one pixel in millimeters allowed to calculate the droplets diameter in this scale.

Figure 2.23: Real image of the reference (to the left), a processed image of the reference (to the right).

To calculated the impact velocity, a function was added to the algorithm that found the centroid of the object. This function allowed to know the position of the object in the image matrix. For this calculation, two images were necessary given that two positions were needed and the difference between these positions allowed to calculate the traveled distance of the droplets.

Figure 2.24: Processed image of a droplet fall.

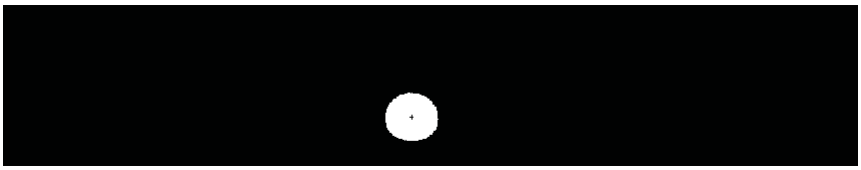

Figure 2.25: Processed image of a droplet before impact.

Through the centroid position of figure 2.24 and figure 2.25, the distance between the droplets position is calculated. Knowing the distance, a time period was needed to calculate the impact velocity. The time period was calculated through the camera's frame rate. Given that the frame rate was $10000fps$, then, 100 µs pass between each frame. In the case of this study, 5 frames are used between the two images, so, the time period is 500 µs. Having the time period and the traveled distance it was possible to calculate the impact velocity of the droplet.

For this work the maximum error for the droplets diameter calculation was considered to be half of the pixel value [25]. So the maximum error obtained for the droplets diameter is 20.3 µm. For the impact velocity, the error value was obtained by dividing half of the highest pixel value for the time period, so the maximum error obtained for the impact velocity calculation is $0.0406\ m/s$.

With a crossflow, the same image processing was used, although in this case two coordinates of the centroid were obtained. It was important to find out how many pixels the droplet moved horizontally and vertically. This allowed the separation of the two components of velocity that were needed for the study. Having the horizontal (U_x) and vertical velocity (U_y), the droplets absolute velocity of impact (U_a) was obtained calculating the resulting vector module and figure 1.2 represent the coordinate system and the velocity components mentioned. The impact angle (θ) was also calculated and it is also represented in the figure.

Chapter 3

Results and Discution

This section details the results obtained in the experimental study. First, it is presented the phenomena observed in this work. Then, some results of the droplet characteristics are presented. The impact conditions differ so, the results and discussion are presented first for the normal impact and then for the impact with a crossflow. A comparison with the transition criteria shown in the literature review is also made and in the end, a summary comparing all the variables is made.

3.1 Phenomena Visualization

There are a variety of phenomena that can be encounter by studying droplet impact. First, were identified the various impingement regimes of the droplet for the study conditions.

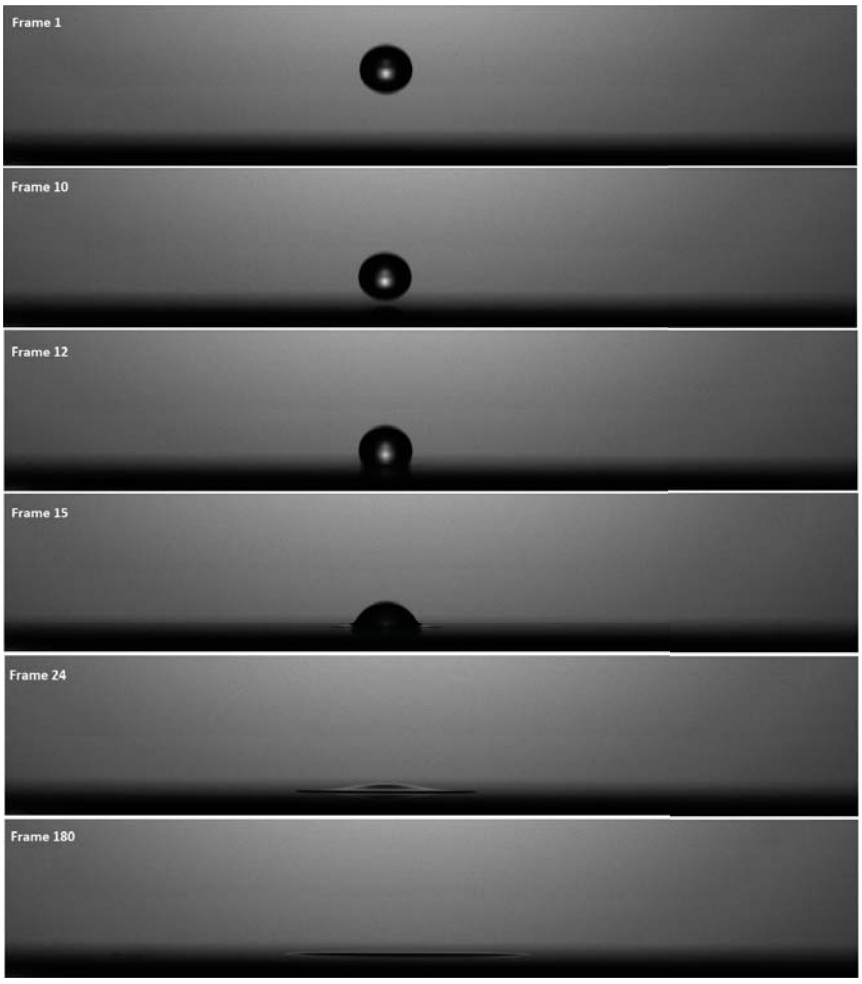

Figure 3.1: A droplet impinging onto an aluminum plate for a $75\%\ JF$ - $25\%\ HVO$ mixture ($D_0 = 3.06mm$;$Re = 4967$;$We = 825$;$La = 29912$).

Figure 3.1 shows a sequence of images that represent the impact on a dry surface. Frame 12 shows the moment of the droplet's impact, and no secondary atomization occurs. Through the observation of the following frames, the boundary condition seen is spread, and occurs when the droplet impacts on a surface with moderated velocity and spreads out to form a wall film. After reaching the maximum spread diameter the wall film recoils towards the center of the droplet (receding stage).

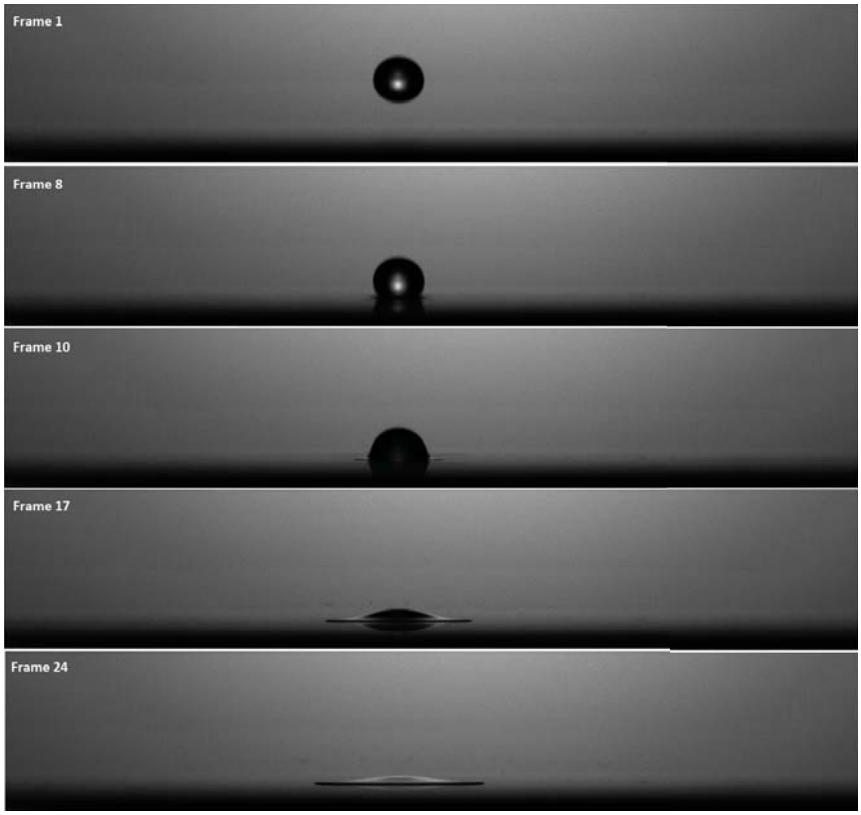

Figure 3.2: A droplet impinging onto an aluminum plate for a 50% JF - 50% HVO mixture ($D_0 = 3.07mm$;$Re = 3863$;$We = 798$;$La = 18708$).

The boundary condition called prompt splash is displayed in figure 3.2. This phenomenon occurs for high Reynolds numbers and is characterized by the formation of smaller droplets when the droplet impinges with the surface at the beginning of the spreading phase (Frame 8). In the next frames are shown the spreading of the droplet, and in frames, 10,17 and 24 the secondary droplets formed by the impingement are observed.

In figure 3.3 is presented the fingering phenomenon. Frame 5 shows that splash does not occur when the droplet impacts on the surface, instead the spreading phase begins. The fingering phenomenon occurs when the lamella formed has surface perturbations that extended radially creating what is called 'fingers' [1]. In frames 13 to 55 it is possible to observe the occurrence of this phenomenon. In the spreading phase, an outer rim was formed and these fingers were formed in this rim. In some cases when the lamella reaches the maximum diameter, these 'fingers' separate from the lamella creating what is called satellite droplets [26]. After the lamella reached the maximum diameter the receding stage began and the droplet recoiled (frame 73).

Figure 3.3: An H_2O droplet impinging onto an aluminum plate ($D_0 = 4.06mm; Re = 15588; We = 828; La = 293454$).

An H_2O droplet impact with a crossflow is display in figure 3.4. In this sequence, a variety of phenomena is presented. The crossflow is applied to the left in this image. Frames 1 and 7 shows that the crossflow causes the droplet to deform. Frame 8 displays a prompt splash, however, frame 11 also shows the creation of a crown-like shape. However, in this case, a crown splash does not occur. This crown is formed by the interaction of the crossflow and the impact of the droplet. The outer rim, formed after impact, created a crown-like shape, and, when the maximum diameter was reached, broke, creating smaller droplets (secondary atomization). Through frame 19, 22, 29 and 40, was noticeable that the crossflow created an upwards movement that elevated the secondary droplets, this is shown comparing the left side and the right side of the figure.

Figure 3.5 shows a droplet breakup phenomenon. Frames 7 and 11 shows that the droplet began to suffer deformation by interacting with the crossflow. After this deformation, the droplet was flattened (frame 17) and began to form a bag (frames 29 to 37). In this bag was also seen the formation of a plume, so this phenomenon is a multimode (bag/plume) breakup [27]. This phenomenon is constituted by three main components, the droplets' bag, ring, and plume. The ring is the thicker part of the perimeter of the bag, and the plume is the small droplet inside the bag. In frame 38 the bag breakup stage occurs, leaving the ring and the plume still intact (frame 42). Only in frame 47, the breakup phenomena was completed when the ring and the plume also break up. This phenomenon was not studied in the present work.

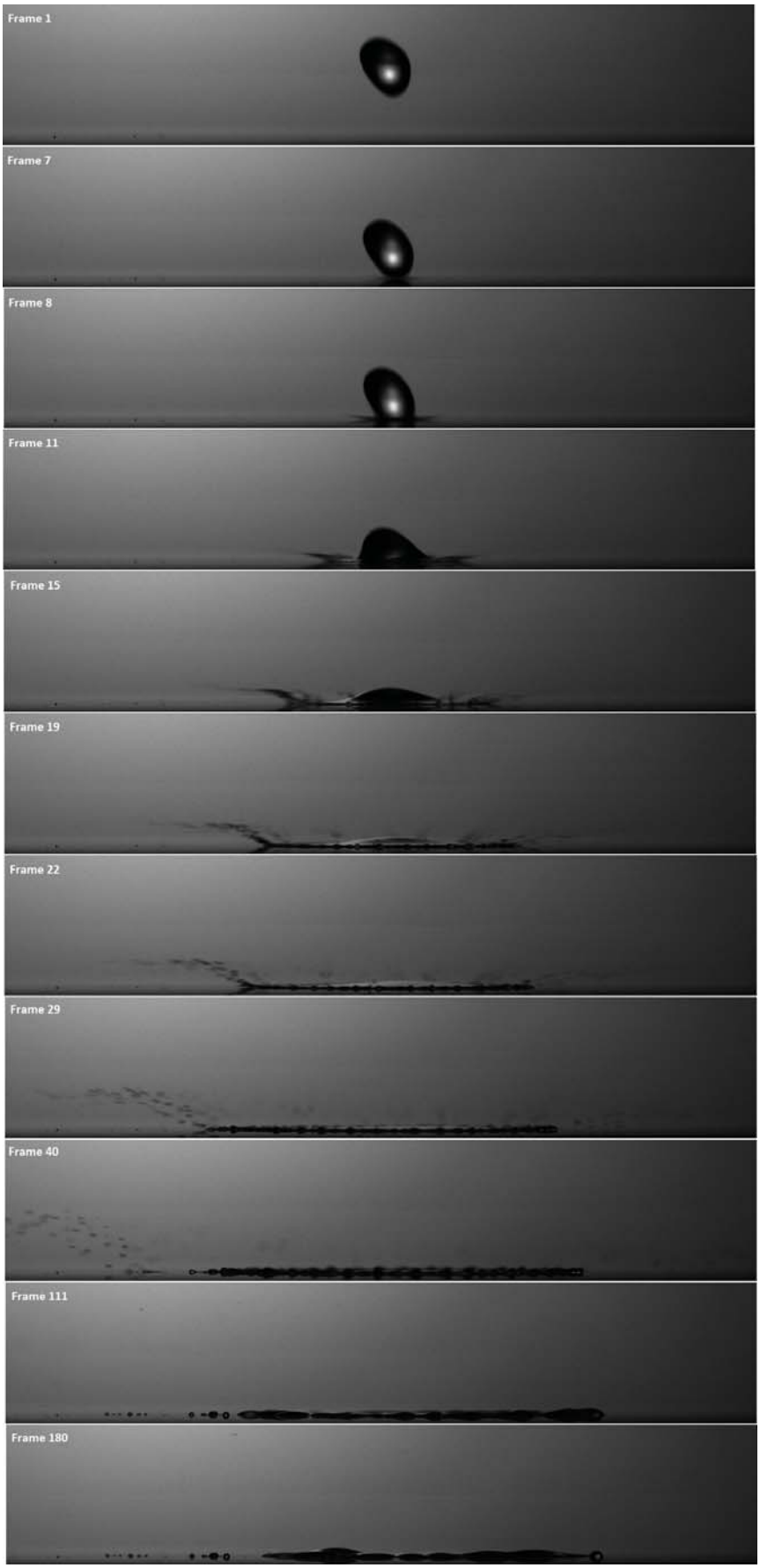

Figure 3.4: An H_2O droplet with $4.06\ mm$ original diameter impinging onto an aluminum plate in a crossflow of $7\ m/s$ ($Re_a = 18618; We_a = 1181; La = 293454$).

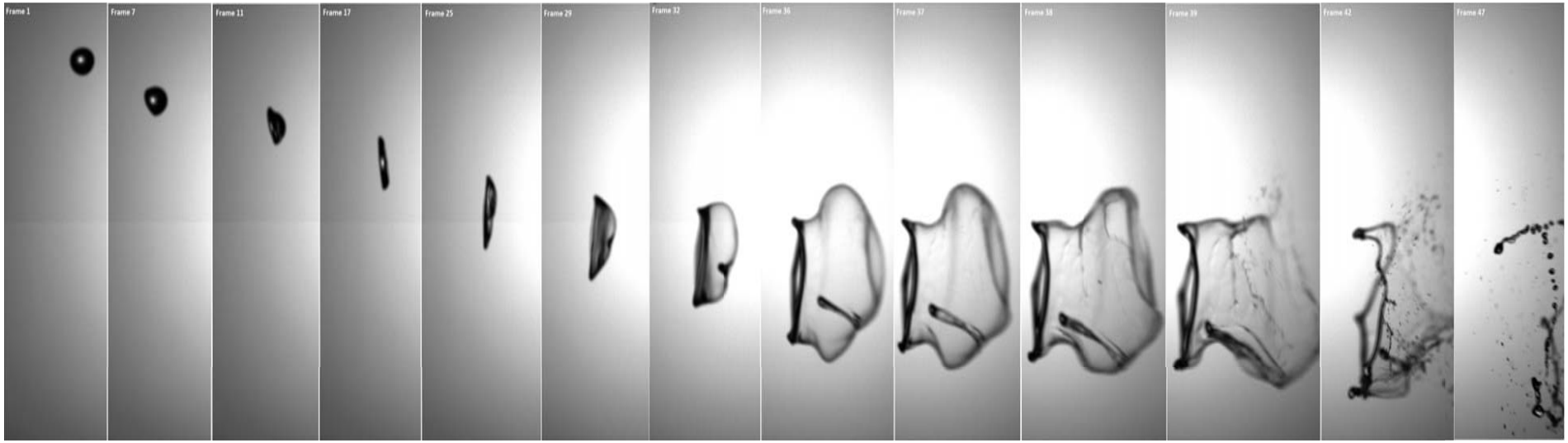

Figure 3.5: An $100\ \%\ JF$ droplet with $3.02\ mm$ original diameter sufering aerodinamic breakup in a $10m/s$ crossflow.

3.2 Splash/Non- Splash Threshold Analise

3.2.1 Normal Impact

The difference between deposition and splash its considered here to be the minimum interval obtainable with the experimental facility. The impact velocity, droplet size, and dimensionless numbers will be presented in this section. Table 3.1 presents the results obtained for a droplet impact without the influence of a crossflow (normal impact).

The results suggest that there is not a definitive property that defines the regime transition. It is possible to observe that all the characteristics of the mixtures presented so far have some relevance for this transition. The density value of the substances seem to influence the droplet size, the higher the density value was, the larger the droplet would be. For the mixtures, it was needed a higher velocity so the transition between deposition and splash could occur comparatively to $100\%\ JF$. The surface tension and density values are almost constant for these mixtures. So, this suggests that the viscosity might be responsible for this differences.

Comparing H_2O to the remaining results, it is noticed that this fluid presents a different range of all variables study. It seems that all thermophysical properties influence the impact outcome. To be able to compare these properties between the mixtures and H_2O it would be of interest to study the impact phenomena with the same droplet diameter.

Table 3.1: Results obtained for normal impact.

	100% JF		75%JF - 25%HVO		50%JF - 50%HVO		H_2O	
	Deposition	Splash	Deposition	Splash	Deposition	Splash	Deposition	Splash
U_0 $[m/s]$	2.03	2.12	2.94	3.01	2.70	2.84	3.86	4.01
Re	4361	4572	4966	5075	3671	3863	15588	16211
We	390	429	825	861	720	798	828	898
Oh$\times 10^3$	4.528		5.782		7.311		1.846	
La	48765		29912		18708		293454	
D_0 $[mm]$	3.02		3.06		3.07		4.06	
ρ $[kg/m^3]$	798.3		795.0		792.4		1000	
σ $[N/m]$	0.02537		0.02553		0.02464		0.07280	
μ $[Pa.s]$	0.00112		0.00144		0.00179		0.00100	

As it was mentioned in chapter 1, some authors have proposed some criteria to predict the occurrence of secondary atomization in dry surfaces. These criteria propose an empirical correlation between some dimensionless numbers that describe the splash/non-splash boundary.

The boundary line proposed by Bai and Gosman [3] is presented in equation 1.6. The coefficient A (shown in table 1.2) depends on the surface roughness. In the present work, the surface roughness was not measured so it is only known that the impact surface is an aluminum plate that was polished for this experimental study. This plate was considered to be 'smooth' but there was not a specific value known for the surface roughness. According to Range [28], the surface roughness of polish aluminum is 0.1470 µm, and considering table 1.2, A =4534. However, Silva [17] and Rodrigues [29] suggest that the coefficient A, for a 'smooth' aluminum plate, is 2634. So both values of A were applied to the criterion and compared with the experimental results. Equations 3.1 and 3.2 represent the different empirical correlations used.

$$We_c = 4534 \times La^{-0.183} \quad (3.1)$$

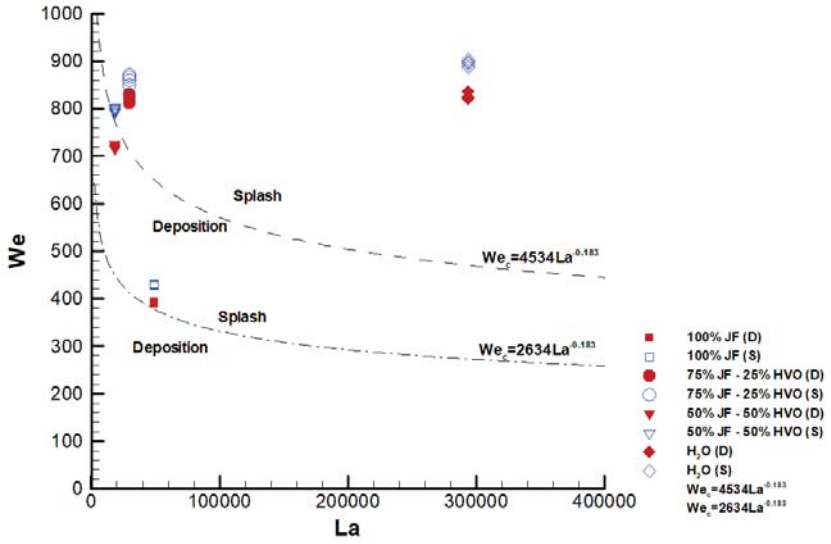

Figure 3.6: Droplets behavior for normal impact compared to Bai and Gosman's [3] criterion with two different A coefficient values.

$$We_c = 2630 \times La^{-0.183} \quad (3.2)$$

The results for the splash/non-splash boundary are presented in figure 3.6. The dashed lines represent equations 3.1 and 3.2 whit the two different A coefficients. The blue data points represent the cases where splash occurred and the red ones where splash was not observed. This figure suggests a difference in the behaviors of the $100\%\ JF$ and H_2O to that of the mixtures. Furthermore, it also indicates that the thermophysical properties like the viscosity, density and surface tension, indeed have some effect in the determination of this threshold. For this normal impact, the $100\%\ JF$ seems to have some proximity to the boundary proposed with the higher surface roughness value. However, the threshold observed in the experimental work does not match to the one proposed if a quantitative evaluation is being made. Despite this, these boundary lines represent a region where the transition between deposition and splash should occur. The $75\%\ JF$-$25\%\ HVO$ mixture has a close proximity to the boundary with the lower surface roughness.This might suggest that the empirical correlation proposed with the lower surface roughness, could be used to predict the transition criteria for the mixtures.

Mundo et al. [4], indicated a different criterion for the boundary line between the phenomena. As it was mentioned before, equation 1.7 translates the boundary line proposed by this author. Figure 3.7 presents the experimental data compared to that boundary and was observed that all of the experimental results were obtained in the splash area. Once again, if a quantitative evaluation is made none of the results match with the empirical correlation. One of the reasons for this might be that the experimental facility used by Mundo et al. [4] had a rotating disc as the impact surface. This means that the effective collision angle might not be the same, giving a possible explanation for this difference. However, is observable a tendency line in the results and some similarity to the empirical correlation proposed. So, if this transition criterion adjusted to the experimental results it could be used to predict the impact phenomenon.

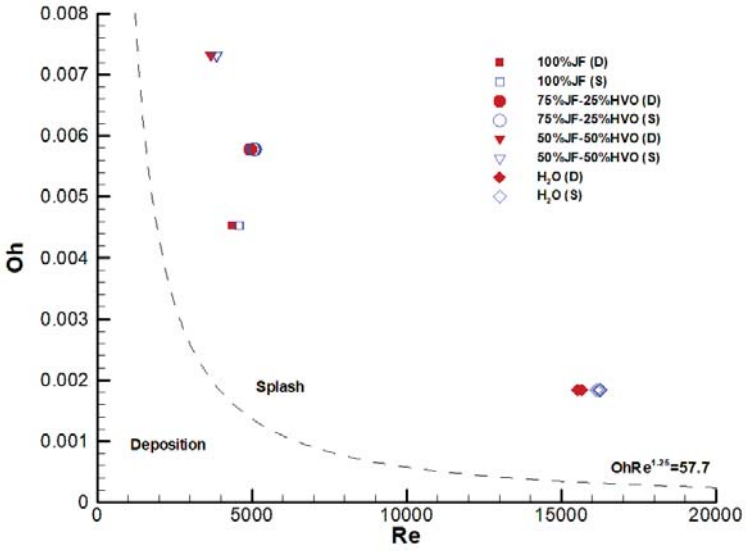

Figure 3.7: Droplets behavior for normal impact compared to Mundo et al. [4] criterion.

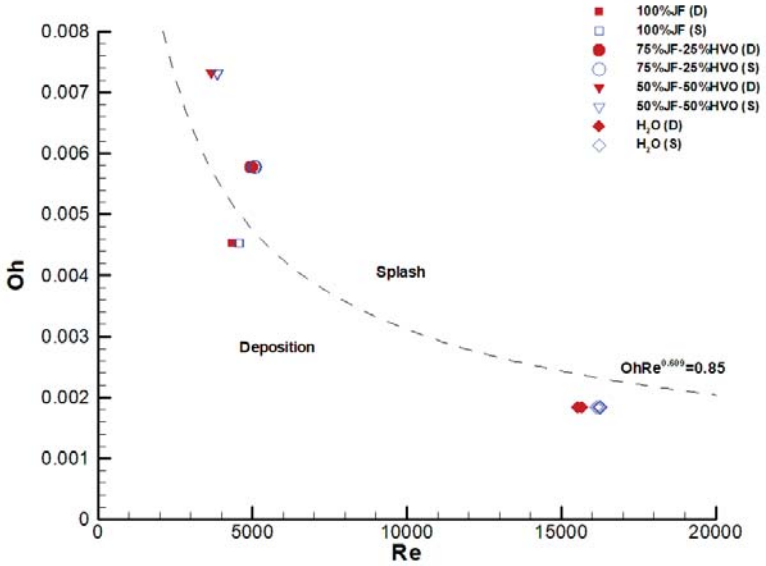

Figure 3.8: Droplets behavior for normal impact compared to Randy et al. [5] criterion.

Randy et al. [5] criterion (figure 3.8) seems to give the better correlation if all substances are considered. Despite the fact that the results from $100\%\ JF$ and H_2O are found in the deposition area and the mixtures in the splash area, there is an overall proximity to the boundary line suggested. So, this criterion may be used for finding the limit between deposition and splash.

All of the criteria presented before suggesting an empirical correlation that could be used to predict the behavior of the droplets for all the substances studied. Mundo et al. [4] correlation look to be the one that differs more from the behavior observed but as it was mentioned, it could be adjusted with further experimental studies. Randy et al. [5] used an aluminum disk with a mean surface roughness of less than $10\ nm$ which could explain the proximity of

the experimental data with this correlation. However, to be able to conclude this, it would be necessary to measure the surface roughness of the aluminum plate of the present work. This is also supported by what was proposed by Bai and Gosman [3], because two values of the surface roughness were used and by observing figure 3.6 is possible to see that Bai and Gosman's correlation could potentially predict the behavior for the mixtures.

3.2.2 Impact with Crossflow

In this section, the same characteristics of the droplets will be presented. However, the droplets impact was studied with the influence of a crossflow. Some authors believe that the droplet impact behavior will be affected by the impact angle. In this case, the impact angle (θ) was defined as the angle formed between the impact surface and the resulting velocity vector (absolute velocity) of the droplets velocity components (figure 1.2). The following results show that the impact angle and the impact velocity were affected by the crossflow. Therefore, the following data will present two types of velocity, namely the absolute vector of velocity, or absolute velocity (U_a) and the vertical impact velocity (U_y). The absolute velocity was calculated from the two velocity components obtained in the image analysis. These results will be divided into sections depending on the crossflow velocity.

3.2.2.1 7 m/s

Table 3.2: Results obtained for the droplets impact with a $7\ m/s$ crossflow.

	100% JF		75%JF - 25%HVO		50%JF - 50%HVO		H_2O	
	Deposition	Splash	Deposition	Splash	Deposition	Splash	Deposition	Splash
U_y $[m/s]$	1.92	2.02	2.73	3.39	2.56	2.99	4.00	4.60
U_a $[m/s]$	2.21	2.29	2.86	3.50	2.73	3.14	4.01	4.61
Re_y	4139	4359	4611	5720	3478	4059	16169	18590
Re_a	4760	4928	4834	5903	3706	4264	16226	18618
We_y	351	390	711	1094	646	881	891	1178
We_a	465	498	781	1165	734	972	897	1181
θ [º]	60.4	62.2	72.6	75.7	69.8	72.1	85.2	86.9
Oh$\times 10^3$	4.528		5.782		7.311		1.846	
La	48765		29912		18708		293454	
D_0 $[mm]$	3.02		3.06		3.07		4.06	

The data described in this section will present the limit were splash was first observed. Although, contrarily to the previous section, the data for the deposition case is not the one immediately before splash occurs. Instead, the limit used here is for the conditions where splash first occurs in the normal impact. In this way, besides the comparison between the characteristics in the threshold, the effect of the crossflow in this characteristics was also noticed. Table 3.2 presents the results obtained in this experimental study. The results presented show the difference between the different velocities vectors used.

Results show that the impact angle increases with the increase of the droplets impact velocity, however, the vertical velocity also increases, which might suggest that when the droplet impact velocity was higher the effect of the crossflow in the droplet was diminished. The splash phenomenon seems to require higher impact velocities for the H_2O and the $75\%\ JF$-$25\%\ HVO$ mixture for splash to occur. As before, more then one thermophysical property seems to define the cause for splash occurs. The same criteria were applied in this case and figures 3.9 and 3.10

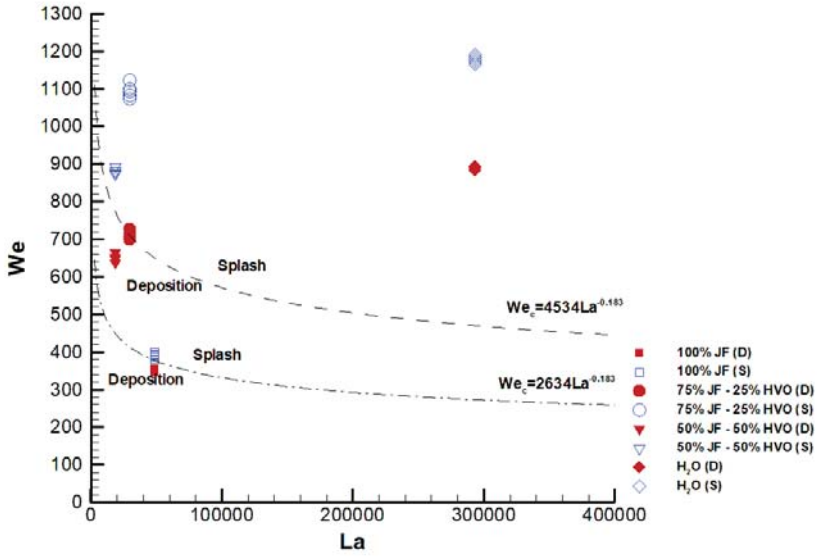

Figure 3.9: Droplets behavior for impact with crossflow relating to its vertical impact velocity compared to Bai and Gosman's [3] criterion.

represent the Bai and Gosman criterion for the results considering the vertical velocity and the absolute velocity respectively. The figures imply that possibly the separation of the vectors of velocity could be helpful, since figure 3.9 shows that the data have a closer approximation to the empirical correlation in the vertical velocity case. Nevertheless, this might only happen because the data used to develop the criterion by Bai and Gosman did not account for a crossflow, instead, it was only used results from what was considered here to be a normal impact.

Mundo et al. criterion [4], shown in figures 3.11 and 3.12 , seems to not give a good correlation for the results obtained. Considering that every point of the results is presented in the criterion splash area. Although, if a trend line was created with the results of the present study it would be almost parallel to the one proposed. This criterion also considers two velocity components, but the rotation of the impact surface is the variable which determines the collision angle and the impingement velocity. A possible explanation for this difference could be the velocity component provided by the impact surface. It had a different direction from the one used in this experimental study. Other possible explanation could be the surface roughness of the impact surface. For this study, this variable was significantly smaller than the one used to create the criterion.

Randy et al. [5] correlation seems to be the closer boundary line if all the substances are considered. However, observing fig 3.14 and figure 3.13, it was noticed that the H_2O almost does not vary for both cases of velocity. In the case of the $100\%\ JF$, it can be seen that there is a close proximity to the boundary if the absolute velocity is used. For the mixtures, vertical velocity has a better association with the empirical correlation.

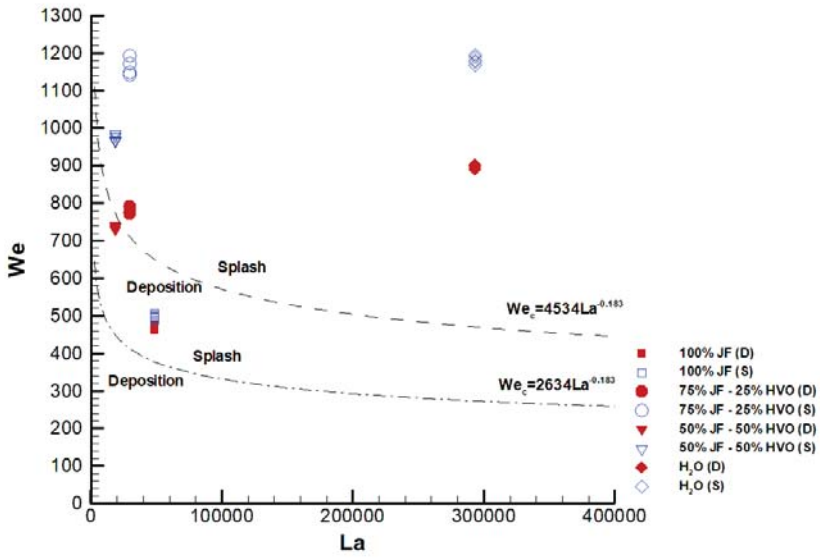

Figure 3.10: Droplets behavior for impact with crossflow relating to its absolute impact velocity compared to Bai and Gosman's [3] criterion.

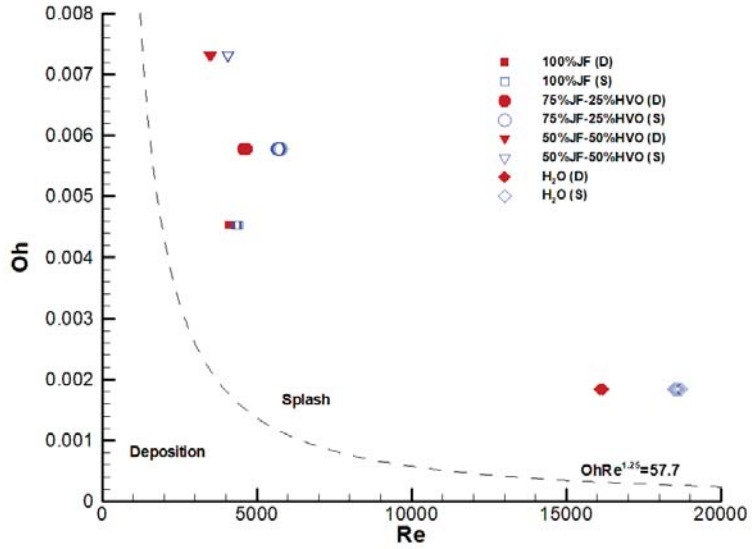

Figure 3.11: Droplets behavior for impact with crossflow relating to its vertical impact velocity compared to Mundo et al. [4] criterion.

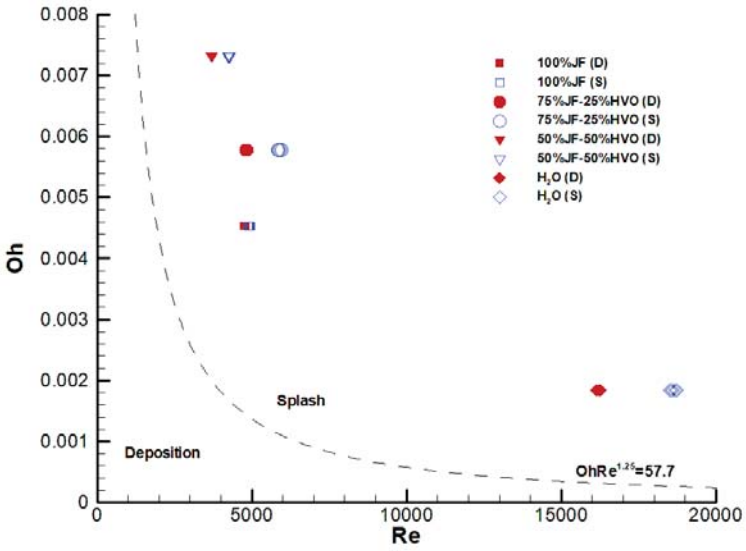

Figure 3.12: Droplets behavior for impact with crossflow relating to its absolute impact velocity compared to Mundo et al. [4] criterion.

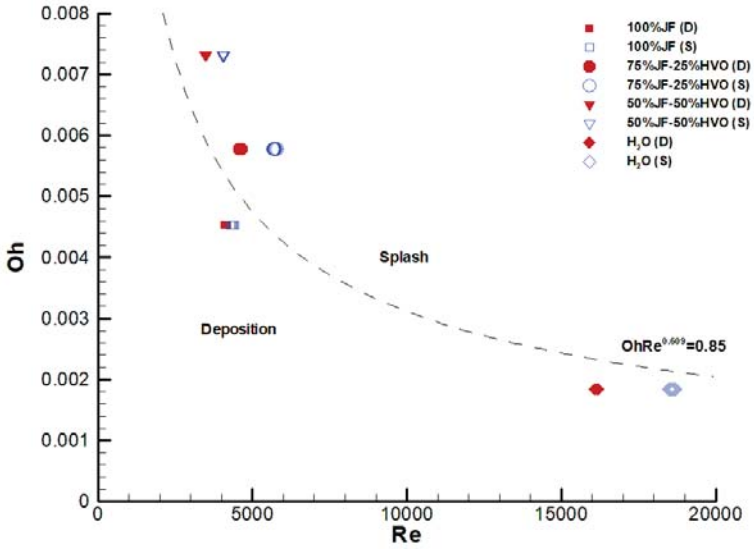

Figure 3.13: Droplets behavior for impact with crossflow relating to its vertical impact velocity compared to Randy et al. [5] criterion.

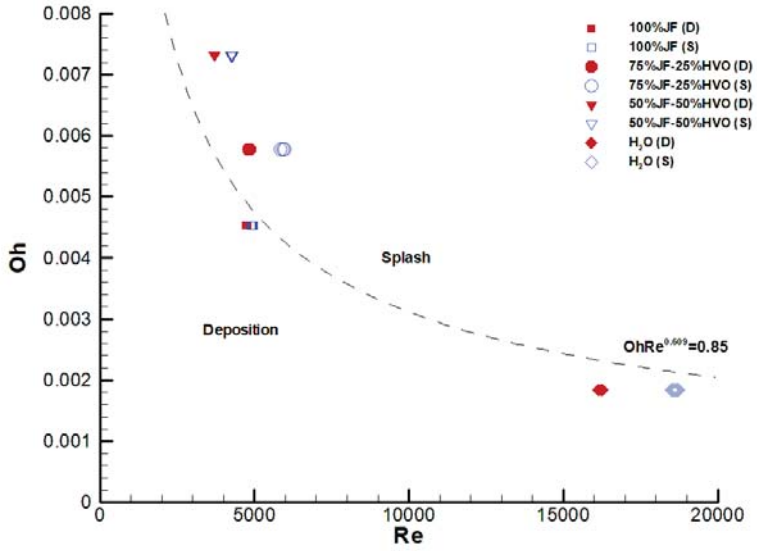

Figure 3.14: Droplets behavior for impact with crossflow relating to its absolute impact velocity compared to Randy et al. [5] criterion.

3.2.2.2 10 m/s

The crossflow velocity was increased to $10m/s$. For the $100\%\ JF$, $75\%\ JF$-$25\%\ HVO$ and 50% JF-$50\%\ HVO$ aerodynamic breakup occurred. So, they were not studied beyond this point. The H_2O did not present aerodynamic breakup and the impact characteristics were studied. The droplets impact velocity varied with the height from where the droplet was launched. Due to limitations in the experimental facility achieving the maximum height, the splash phenomenon was not observed. Table 3.3 shows the results for the H_2O. L_1 is the limit used in the 7 m/s case where splash was observed and L_2 is the limit for the maximum height obtainable with this experimental facility.

Table 3.3: Results obtained for the droplets impact with a $10\ m/s$ crossflow.

	H_2O	
	L_1	L_2
U_y [m/s]	4.50	4.70
U_a [m/s]	4.56	4.76
Re_y	18197	19022
Re_a	18433	19232
We_y	1037	1134
We_a	1134	1159
θ [°]	80.8	81.6
Oh$\times 10^3$	1.846	
La	293454	

3.3 Summary

The results obtained suggest that the thermophysical properties of the substances influence the droplet impact phenomenon. As it was already mentioned more than one property seems to have a correlation with the impact outcome. It was shown that the impact velocity, for the

Table 3.4: Comparison between Normal Impact (NI), where splash occurs, and Crossflow Impact (CI), where deposition occurs.

	100% JF		75%JF - 25%HVO		50%JF - 50%HVO		H_2O	
	NI	CI	NI	CI	NI	CI	NI	CI
U_y $[m/s]$	2.12	1.92	3.01	2.73	2.84	2.56	4.01	4.00
U_a $[m/s]$		2.21		2.86		2.73		4.01
Re_y	4572	4359	5075	4611	3863	3478	16211	16169
Re_a		4760		4834		3706		16226
We_y	390	390	861	711	798	646	898	891
We_a		465		781		734		898

same outcome, varies in the same manner for a normal impact (NI) and for a crossflow impact (CI). This does not mean that the crossflow or the impact angle had no effect on the splash/non-splash boundary.

Table 3.4 presents the results for the same initial parameters for NI and CI. However, the impact conditions differ. This table presents the results for when splash occurs for NI and deposition for CI. Trough this table its observable that the crossflow affects the outcome of the droplet impact. For the same initial condition, both velocity components are often lower for the CI. This suggests that the crossflow decreases the impact velocity. Nonetheless, for $100\%\ JF$ and H_2O, this was not observed. In the case of $100\%\ JF$, the absolute velocity was higher. This might suggest that the impact angle affect the outcome of the droplets impact since splash was not observed for CI. Also, the results show that the tangential component to the surface is larger for droplets with smaller diameters, which can be an explanation for the increase of the impact velocity. Droplets with smaller size are more quickly affected by the crossflow. The analysis of the H_2O case might support this since the impact velocity for this fluid did not have a significant variation, neither comparing the type of impact nor the two velocity components. This fluid had the biggest droplet size suggesting that the crossflow velocity was not enough to influence the droplet impact. Other explanation could be that the crossflow cause deformation in the droplet delaying the splash phenomenon.

Table 3.5: Comparison between Normal Impact (NI) and Crossflow Impact (CI), where splash occurs for both cases.

	100% JF		75%JF - 25%HVO		50%JF - 50%HVO		H_2O	
	NI	CI	NI	CI	NI	CI	NI	CI
U_y $[m/s]$	2.12	2.02	3.01	3.39	2.84	2.99	4.01	4.60
U_a $[m/s]$		2.29		3.50		3.14		4.61
Re_y	4572	4359	5075	5720	3863	4059	16211	18590
Re_a		4928		5903		4264		18618
We_y	390	390	861	1094	798	881	898	1178
We_a		498		1165		972		1181

Table 3.5 presents the results for the parameters where splash occurred for NI and CI. In this case, both the initial parameters and impact conditions differ. These results suggest that crossflow delays the occurrence of splash. This is also supported by observing table 3.3 where the crossflow had a higher velocity and for the same initial parameters the impact velocity decreased. For the majority of the substances, both the absolute velocity and the vertical velocity had to increase so the splash phenomenon could be observed, except for the $100\%\ JF$ case. In the last case, only the absolute velocity was higher than in the NI. This could suggest that the absolute velocity has a bigger influence on the impact outcome. Still, the $100\%\ JF$ is the only

substance where this happens. The remaining results suggest that the vertical velocity needs to be higher in a CI than in an NI for the same outcome to occur. Further studies can be made to better conclude which of the velocity components has a higher influence. Excluding the 100% JF, the experimental data suggests that the vertical velocity could have a bigger roll in the impact outcome.

For the same crossflow velocity, the impact angle increases with the increase of the vertical impact velocity. The vertical velocity component becomes big enough to almost nullify the crossflow influence in this variable. Increasing the crossflow velocity to $10m/s$, corroborated this hypothesis. The velocity vector provided by the crossflow was increased, the initial parameters were kept the same and it was observed that the impact angle decreased.

Referring to the transition criteria, although Mundo et al. [4] used two velocity components in his experiment for the development of his empirical correlation, the experimental results presented here do not quantitatively match the boundary suggested. This was observed for both impacts (NI and CI), although, if a trend line was made for the results of the present work, it would be almost parallel to the one proposed in this criterion.

Randy et al.[5] seem to give a better approximation to all substances. This approximation could also be explained by the fact that these authors used an aluminum disk with a surface roughness of approximately $10nm$ which could also substantiate the surface roughness values used in the Bai and Gosman's [3] criterion . One point that does not seem to correlate with the remaining criteria is for 100% JF. Contrarily to mixtures, the absolute velocity is in the closest proximity to the boundary.

By observing the results comparing with Bai and Gosman's [3] boundary, the data highlights the importance of separating the velocity components. A closer proximity to the limit proposed is obtained by vertical impact velocity case. For a higher value of the surface roughness (lower A coefficient), the 100% JF matched quantitively with the limit. Despite this, mixtures had a better approximation to the limit with the lower value (higher A coefficient) of the surface roughness.

This experimental study suggests that the surface roughness, the thermophysical properties, the impact angle and the crossflow could influence the impact outcome. Randy et al.[5] criteria could possibly be used to predict the impact outcome of the droplet given that all the substances are close to the boundary line proposed. Since all four substances have different thermophysical properties and the boundary line is close in all of them sustains the possible use of this empirical correlation.

Chapter 4

Conclusions

Trough the years a growing attention is given to the study of sprays and droplets impingement processes. This studie allow to studie the impingement processes and thermophysical properties of the jet fuel, water, and the mixtures.

The goal of this work was to study the deposition/splash threshold of the droplets impingement on a dry surface for four different substances. Two types of impact were used, normal impact and crossflow impact. To accomplish this, an experimental facility was designed to allow variations in impact velocity of the droplet.A wind tunnel was built to provide a crossflow and in this way evaluate the influence of the crossflow in the impingement phenomena.

It was shown that the surface tension, viscosity, and density influenced the droplet size and impact phenomena. The crossflow seems to have some significance on the droplets impact. The same initial parameters had different outcomes regarding normal impact and crossflow impact. For the different crossflow velocities impact was not always observed. Therefore those cases were not studied. For 10 m/s all substances, except H_2O, suffer aerodynamic breakup, the same happened for all four at 15 m/s. The droplets velocity were divided into two components to study the influence of each one in the impingement process. The results show that depending on the crossflow velocity, the components behaved in different ways. For the majority of the substances, the absolute velocity and the vertical velocity had to be increased in order to observe the splash phenomenon. The results suggest that the vertical velocity needs to be higher in a crossflow impact than in an normal impact, for the same outcome can occur. Despite this, for 10 m/s, vertical velocity and absolute velocity decreased, which could be related to a higher influence of the crossflow. For the same crossflow velocity, the impact angle increases with the increase of the vertical impact velocity. Based on the results, it seems that when vertical velocity component becomes high enough, it can almost nullify the crossflow influence in this variable.

Furthermore, the results were compared to the transition criteria mentioned in the literature review. This highlighted another variable in the impact outcome, the surface roughness. The surface roughness was not measured for this experimental work delimitating the comparison with other studies. Comparing the results with these criteria, it suggests that Randy et al.[5] boundary line gives a better overall proximity to experimental data. However, Bai and Gosman's threshold matched with the mixtures results. The vertical velocity results seem to give the tightest approximation to the boundary line.

In conclusion, the influence of the biofuel was clearly noticed in the results. The mixtures presented different behaviors compared to the jet fuel and the control substance.

In order to further investigate the subject, a study of a wider range of Webber and Reynolds numbers should be performed. This may allow establishing an empirical correlation to predict the mixtures droplets behavior. Also, it would be interesting evaluate droplets behavior with the same size for the four different mixtures. A research on multiple droplets impacts could be done, so the dynamic between droplets could be observed. It could also be a point of

interest to add different mixture ratios to this study, in order to obtain a deeper understanding of the biofuel influence. Also, the aerodynamic breakup phenomenon should be investigated, aside with the size and distribution of the secondary droplets. In future studies, the surface characteristics could be highlighted. Surface roughness, temperature, and surface angle are variables of interest, so further comparisons can be added to this work.

Bibliography

[1] A. Yarin, "Drop Impact Dynamics: Splashing, Spreading, Receding, Bouncing…," *Annual Review of Fluid Mechanics*, vol. 38, no. 1, pp. 159–192, 2006. xi, 2, 4, 24

[2] A. Moita and A. L. N. Moreira, "Influence of surface properties on the dynamic behavior of impacting droplets," 2018. xi, 4

[3] C. X. Bai and A. D. Gosman, "Development of a Methodology for Spray Impingement Simulation," *SAE Paper 950283,Society of Automotive Engineers*, 1995. xi, xii, xiii, 2, 5, 28, 29, 31, 32, 33, 37

[4] C. Mundo, M. Sommerfeld, and C. Tropea, "Droplet-wall collisions: Experimental studies of the deformation and breakup process," *International Journal of Multiphase Flow*, vol. 21, no. 2, pp. 151–173, 1995. xii, 3, 4, 29, 30, 32, 33, 34, 37

[5] R. L. Vander Wal, G. M. Berger, and S. D. Mozes, "The splash/non-splash boundary upon a dry surface and thin fluid film," *Experiments in Fluids*, vol. 40, no. 1, pp. 53–59, 2006. xii, 6, 30, 32, 34, 35, 37, 39

[6] R. Rioboo, C. Tropea, and M. Marengo, "Outcomes From a Drop Impact on Solid Surfaces," *Atomization and Sprays*, vol. 11, no. 2, p. 12, 2001. xiii, 1, 4

[7] B. Pizziol, "Design and Experimental Characterization of an Air-Assisted, Impinging-Jets Atomizer for Aeronautical Applications with Biofuel," Master Thesis, Politecnico Di Milano, 2017. 1

[8] R. L. Vander Wal, G. M. Berger, and S. D. Mozes, "Droplets splashing upon films of the same fluid of various depths," *Experiments in Fluids*, vol. 40, no. 1, pp. 33–52, 2006. 2, 6

[9] A. S. Moita and A. L. Moreira, "Experimental study on fuel drop impacts onto rigid surfaces: Morphological comparisons, disintegration limits and secondary atomization," *Proceedings of the Combustion Institute*, vol. 31 II, pp. 2175–2183, 2007. 2

[10] O. Jayaratne and B. J. Mason, "The Coalescence and Bouncing of Water Drops at an Air/Water Interface," *Proceedings of the Royal Society of London Series A-Mathematical and Physical*, vol. 280, no. 138, pp. 545–565, 1964. 3

[11] S. C. Yao and K. Y. Cai, "The Dynamics and Leidenfrost Temperature of Drops Impacting on a Hot Surface at Small Angles," *Experimental Thermal and Fluid Science*, vol. 1, no. 4, pp. 363–371, 1988. 3

[12] A. S. Moita, "Thermal and Fluid Dynamics of Droplet Wall Interactions," Ph.D. dissertation, 2009. 4

[13] C. Mundo, M. Sommerfeld, and C. Tropea, "On the modeling of liquid sprays impinging on surfaces," *Atomization and Sprays*, vol. 8, pp. 625–652, 1998. 4, 5

[14] Z. Levin and P. Hobbs, "Splashing of Water Drops on Solid and Wetted Surfaces: Hydrodynamics and Charge Separation," *Philosophical Transactions of the Royal Society of London*, vol. Vol. 269a„ 1971. 4

[15] C. D. Stow and M. Hadfield, “An Experimental Investigation of Fluid Flow Resulting from Impact of a Water Drop with an Unyielding Dry Surface,” *Proceedings of The Royal Society A: Mathematical, Physical and Engineering Sciences*, vol. 373, pp. 419–441, 1981. 4, 5

[16] H. Zhang, B. Bai, L. Liu, H. Sun, and J. Yan, “Droplet dispersion characteristics of the hollow cone sprays in crossflow,” *Experimental Thermal and Fluid Science*, vol. 45, pp. 25–33, 2013. 4

[17] A. Silva, “Experimental and Numerical Study of Physical Aspects of Fuel Injection Processes,” PhD Thesis, University of Beira Interior, 2007. 4, 5, 28

[18] M. Panão, A. L. N. Moreira, and D. Durao, “Effect of a cross-flow on spray impingement with Port Fuel Injection systems for HCCI engines,” *Fuel*, vol. 106, p. In press, 2012. 4

[19] M. Panão and A. L. N. Moreira, “Experimental characterization of intermittent gasoline sprays impinging under cross flow conditions,” *Atomization and Sprays*, vol. 15, p. 201, 2005. 4

[20] V. Brederode, *Fundamentos de Aerodinâmica Incompressivel*, author’s ed., Lisboa, 1997. 7

[21] R. D. Mehta and P. Bradshaw, “Technical Notes Design Rules for Small low Speed Wind Tunnels,” *The Aeronautical Journal of the Royal Aeronautical Society*, vol. 83, no. 827, pp. 443–449, 1979. 8, 10

[22] R. D. Mehta, “Turbulent boundary layer pertubed by a screen,” *American Institute of Aeronautics and Astronatics Journal*, vol. 23, no. 9, pp. 1335 – 1342, 1985. 8

[23] T. Morel, “Design of Two-Dimensional Wind Tuunel Contractions,” *Journal of Fluids Engineering*, vol. 99, no. 2, pp. 371–377, 1977. 10, 11

[24] B. S. Stratford, “The prediction of separation of the turbulent boundary layer,” *Journal of Fluid Mechanics*, vol. 5, no. 1, pp. 1–16, 1959. 10

[25] C. Tropea, A. L. Yarin, and J. F. Foss, *Springer handbook of experimental fluid mechanics*, 2007, no. 1. 17, 18, 22

[26] C. Stanley, R. Jackson, N. Karwa, and G. Rosengarten, “The Effects of Surface Wettability on Droplet Fingering,” no. December, 2014. 24

[27] Z. Dai and G. M. Faeth, “Temporal properties of secondary drop breakup in the multimode breakup regime,” *International Journal of Multiphase Flow*, vol. 27, no. 2, pp. 217–236, 2001. 25

[28] K. Range, “Influence of Surface Roughness on Liquid Drop Impact,” *Journal of Colloid and Interface Science*, vol. 203, no. 1, pp. 16–30, 1998. 28

[29] C. Rodrigues, “Modelling of a Biofuel Spray Wall Impingement,” Ph.D. dissertation, 2015. 28